LASER SCATTERING AS A TOOL TO DETERMINE THE EFFECT OF TEMPERATURE ON DIATOM AGGREGATION

A Thesis

by

CHARLES EDWARD RZADKOWOLSKI

Submitted to the Office of Graduate Studies of
Texas A&M University
in partial fulfillment of the requirements for the degree of

MASTER OF SCIENCE

August 2010

Major Subject: Oceanography

Laser Scattering as a Tool to Determine the Effect of

Temperature on Diatom Aggregation

LASER SCATTERING AS A TOOL TO DETERMINE THE EFFECT OF TEMPERATURE ON DIATOM AGGREGATION

A Thesis

by

CHARLES EDWARD RZADKOWOLSKI

Submitted to the Office of Graduate Studies of
Texas A&M University
in partial fulfillment of the requirements for the degree of

MASTER OF SCIENCE

Approved by:

Chair of Committee,	Daniel C. O. Thornton
Committee Members,	Sarah Brooks
	Heath Mills
Head of Department,	Piers Chapman

August 2010

Major Subject: Oceanography

ABSTRACT

Laser Scattering as a Tool to Determine the Effect of

Temperature on Diatom Aggregation.

(August 2010)

Charles Edward Rzadkowolski, B.S., Coastal Carolina University

Chair of Advisory Committee: Dr. Daniel C. O. Thornton

Diatoms are estimated to contribute 25% of the primary production on Earth and therefore they play a significant role in the global carbon cycle. Diatom blooms often terminate with the formation of aggregates that sink rapidly from surface waters, affecting the flux of organic carbon from the surface to deep waters and the sea floor. The role of carbon-rich transparent exopolymeric particles (TEP) in aggregate formation as ocean temperature increases has yet to investigated in continuous cultures. I hypothesize that temperature increase can influence the production of TEP, a fraction of total suspended exopolymers. To test the hypothesis, a laser *in situ* scattering and transmissometry instrument (LISST-100X, Sequoia Instruments) successfully counted and sized six individual diatom species in batch culture: *Chaetoceros muelleri*, *Coscinodiscus wailesii*, *Thalassiosira weissflogii*, *Phaeodactylum tricornutum*, *Skeletonema costatum*, and *Skeletonema marinoi* and successfully demonstrated its efficacy in detecting diatom aggregates using *S. costatum*. Four replicate continuous cultures were sampled for particle size distribution (PSD), nutrients, chlorophyll *a*, total

carbohydrates, prokaryote concentration, and TEP at temperatures of 22.5, 27 and then 20 °C. While TEP particles were scarce, acid polysaccharide (APS)-coated *C. muelleri* cells were observed, forming dense webs on the filters. Both carbohydrate per cell and APS area per cell were found to significantly correlate with temperature ($p<0.05$) while significant difference between APS concentration at each temperature was only found between 27 and 22.5 or 20 °C ($p<0.05$). Net changes in PSDs with increasing temperature showed that distributions of relative volume concentration decreased in the smallest size bins and increased in the largest size bins. Our results show that increasing the temperatures of nitrogen-limited *C. muelleri* cultures did not cause increased TEP formation but instead resulted in increased cell-surface coating. Increasing concentration of cell coatings and TEP particles will cause diatoms to aggregate more readily, enhancing their sinking rate away from the ocean surface. Increased ocean temperature has great implications for diatom blooms and other microorganisms, causing greater export of carbon out of the surface waters and potentially altering the microbial loop.

DEDICATION

I dedicate this manuscript to Jennifer Williams, her encouragement and belief in me made it all possible.

ACKNOWLEDGEMENTS

First, I would like to acknowledge the NSF grant OCE 0726369 to DCOT "Effect of temperature on extracellular polymeric substance (EPS) production on diatoms" as its funding made conducting my research possible. Second, I would like to thank Sarah Brooks, Heath Mills, and Dan Thornton for the extensive guidance they've provided me in preparing my research for this thesis. Lastly, I would like to thank Jennifer Williams, Chen Jie, and Stuart Pearce for their advice and continual support along the way.

TABLE OF CONTENTS

Page

Page

LIST OF FIGURES

Page

Page

Page

Page

Page

LIST OF TABLES

Page

1. INTRODUCTION

1.1 Diatom impact and significance

Phytoplankton, including diatoms, contribute to the accumulation of organic carbon in the benthic environment (Billett et al. 1983). The proliferation and subsequent death of phytoplankton blooms, particularly in the spring and fall, directly affect fluxes of carbon from the upper water column as determined through benthic photography and sediment trap analysis (Deuser 1970; De Jonge 1980; Legendre 1990). Although the sources of continuous, and seasonally-variable, deposition of particulate organic carbon (POC) to the sea floor have been determined to be both terrigenic (land-based) and planktonogenic in origin, the planktonic contribution of POC from diatoms can be discretely determined and analyzed (Leventer 1991), leading to the conclusion that diatom blooms alone can impart significant amounts of carbon to the ocean floor (Deuser 1970, Ivanov et al. 2000). The correlation of silica production and primary production has been used in the past to report that diatoms comprise approximately 33% of primary production in the world ocean (Nelson et al. 1995; Treguer and Pondaven 2000). More importantly, the corollary to the conclusion that diatoms contribute largely to this deposition is that through sinking, a diatom population is effectively sequestering carbon from the surface waters and contributing to the biological carbon pump. Studies of the close relationship between mineral ballast of opals or carbonates and POC

This thesis follows the style of *Journal of Phycology.*

(Klaas and Archer 2002; De La Rocha et al. 2008), have increased our understanding of how the settling of phytoplankton acts as vertical pathway for organic carbon (Billett et al. 1983; De La Rocha et al. 2008). With much focus on the role of the oceanic carbon cycle and its implication as a major player in forcing global climate change (Broecker 1982; Omta et al. 2006), the significance of phytoplankton settling becomes more apparent.

1.2 Warming oceans and diatom physiology

Models project, with high probability, a doubling of global atmospheric carbon dioxide and a warming of ocean surface temperature, ranging from 1-1.5 °C before the end of the 21st century (IPCC 2007). Although phytoplankton are found in every ocean basin in the world, temperatures (as well as irradiance and nutrients) can vary widely. Each species can thus be acclimated to an optimum temperature range. There is obvious concern for the impact of temperature change on the physiology of phytoplankton and their ability to adapt. Although species dependent, acclimation responses in diatoms and other phytoplankton can be measured and interpreted directly from chl *a*:carbon (Geider et al. 1997; Behrenfeld et al. 2008, 2009), demonstrating not only an adjustment to metabolism and pigment concentration but also possible changes in intracellular carbon allocation through the exudation of polysaccharides (Geider et al. 1997; Thornton 2002). We do not know how diatoms will allocate carbon in a warmer ocean or how it will affect carbon cycling, such as in the biological carbon pump. Therefore, the role of global sea temperature in the production of carbon exudates begs further investigation.

1.3 Diatom aggregation

Diatoms, as well as other planktonic organisms, exude extracellular polymeric substances (EPS) during normal growth as a result of DIC assimilation. These EPS contribute to the formation of three classes of substances: cell coatings, water-soluble EPS, and transparent exopolymer particles (TEP) (Thornton 2002). There is a need for further research on the dynamic interactions between the accumulation of cell coatings, dissolved EPS, and TEP, with inorganic and organic particles.

It has been estimated that more than 1/3 of the total 45 Pg C of net primary production per annum will sink below the thermocline to be remineralized as CO_2 or become a carbon source for benthic organisms (Falkowski 1998). This flux is strongly coupled with CO_2 drawdown from the atmosphere. While the reason for aggregation remains unclear, the rate of sinking is directly related to the size of the particles. Therefore, aggregation of small particles into large particles enhances the downward flux of organic matter from the surface ocean (Falkowski 1998; Wohlers et al. 2009). Physiological and adaptation-centric reasoning for diatom aggregation has been well-researched and compiled (Thornton 2002). with debate focused between two theories: First, diatom aggregation as a life process step whereby they are active at the surface and, once sunk, retain life to stay in rest (Smetacek 1985) and, second, the explanation that aggregation is a side effect of the production of unused photosynthate in nutrient-depleted waters, resulting in the exudation of EPS (Fogg 1983; Thornton 2002).

While the exact mechanisms behind what drives aggregation of organic material are not known with confidence, successful attempts have been made to compile

hypotheses (Thornton and Thake 1998; Thornton 2002). Thornton and Thake (1998) concluded, based on laboratory experiments with *Skeletonema costatum*, that transferring diatoms from cold to warm water resulted in aggregation while transferring them from warm to cold water caused aggregates to dissociate, without any change in diatom biomass. Furthermore, it was hypothesized that diatoms became more 'sticky' at warmer temperatures (Thornton and Thake 1998). Claquin et al. (2008) showed a significant linear relationship between rise in temperature and TEP production in diatom species investigated (including *Skeletonema marinoi*), with TEP production increasing until each species surpassed maximum growth temperature, at which point production rates decreased quickly.

Although cell stickiness (chance for particle adhesion upon collision) itself is not being investigated in this study, TEP can significantly increase the efficiency at which particles stick together upon collision (Engel 2000). Furthermore, the presence of TEP, can effectively scavenge detritus, zooplankton, and phytoplankton, adding to particle size (Kiørboe et al. 1994; Crocker and Passow 1995; Jackson 1995; Engel 2000; Thornton 2002, 2004; Li et al. 2008; Harlay et al. 2009). TEP-laden particles (marine snow) are implicated as the majority exporter of organic material from the euphotic zone (Passow et al. 2001; Piontek et al. 2009). Recent data indicates that ocean acidification could dissociate TEP particles (Mari 2008). However, other evidence suggests that CO_2-induced global temperature rise could enhance TEP production, altering the upper-ocean carbon flux through aggregation dominated by diatoms (Thornton and Thake 1998; Thornton 2002; Sarthou et al. 2005; Schartau et al. 2007; De La Rocha et al. 2008;

Claquin et al. 2008; Li et al. 2008; Piontek et al. 2009; Wohlers et al. 2009). Consequently, while there is evidence that global climate change in the form of ocean

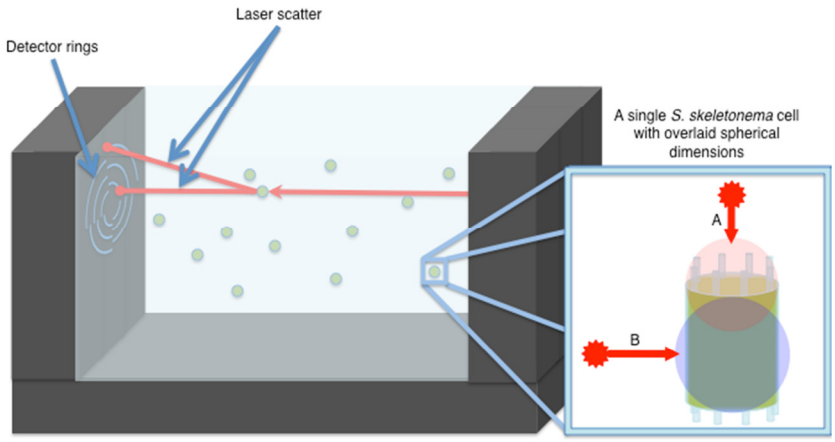

Fig. 1. Simplified figure of the LISST sample chamber. The laser passes through the liquid sample, scattering off suspended particles and is intercepted by the detector rings. The cell-view pane shows a single cell's possible spherical dimensions (A or B) depending on its orientation to the laser path.

acidification and temperature increase will affect the oceanic carbon cycle, the magnitude of these changes, and implications for the efficiency of the biological carbon pump are largely unknown.

1.4 The LISST-100X-C particle size analyzer

The laser in situ scatterometer and transmissometer (LISST) (Sequoia Instruments, Bellevue, WA) is a self-contained particle size analyzer developed and tested to quantify sediment transport *in situ* without perturbation of native distributions (Gartner 2001). The instrument operates by detecting the scattering of a 5 cm light path laser (λ = 670 nm) by suspended particles onto 32 logarithmically spaced detector rings (median ring values of 2.72-460 μm). A particle detected by a ring is assumed to be

spherical in shape and assigned an equivalent spherical diameter (see Fig. 1). Its volume is calculated along with the volumes calculated from each of the other detector rings to produce a particle size distribution (PSD) where peak heights are represented by the volumes detected at each size bin. For example, a suspension of spherical particles of the same diameter would be detected by rings straddling the particles' corresponding diameter producing a distinct peak on the resultant PSD.

Should a particle with different major and minor axis dimensions (e.g. long and narrow) pass in front of the laser, each axis is assumed to correspond to the diameter of a spherical particle, resulting in the detection and display of two distinct peaks on the PSD

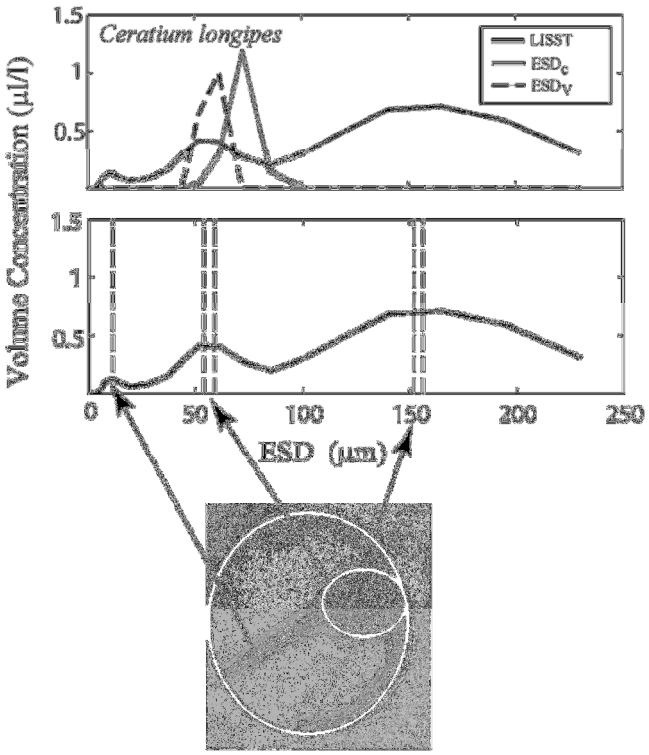

Fig. 2. Adapted from Karp-Boss et al. (2007). The bottom two panels represent Karp-Boss' interpretation of potential spherical targets detectable by the LISST of dinoflagellates *Ceratium longipes* and the resultant particle size distribution (PSD) with peaks corresponding to each spherical diameter.

as each cross-section is scattered by the laser (Fig. 2). Therefore, complicated geometric shapes should possess unique LISST-generated PSD based upon the cross-section scattering the laser. While diatom species can be broadly categorized as either pennate (two cones end-to-end) or centric (cylinder), they can vary considerably in length (from <10 to >200 μm), their ability to form chains, and their possession of accouterments in the form of spines. Therefore, whatever diatom features are within the detectable size range of the LISST should lend to producing a unique spectra that can be used to differentiate between species.

1.5 Study objectives

The LISST-100X has only recently become a potential instrument for identification and quantification of biological entities (Serra et al. 2001; Karp-Boss et al. 2007; Rienecker et al. 2008) so its ability to distinguish between different diatoms and also provide quantifiable data on any changes in that population (e.g. aggregation) needs to be determined.

My main hypotheses for these experiments are:

1. Diatoms possess geometric shapes that can be characterized by a laser-based sediment particle analyzer (LISST-100X).

   Approach: The LISST-100X fits spherically estimated spherical particle volumes into logarithmically spaced size bins (Gartner 2001; Agrawal et al. 2008) so the determination of each diatoms distinct PSD can be achieved based upon peak height and peak position.

2. Increased temperature affects increased exudate release, in the form of TEP, in nitrogen-limited diatom cultures, leading to the formation of diatom aggregates.

   Approach: Nitrogen is widely considered to be the major limiting nutrient in coastal marine ecosystems (Howarth and Marino 2006). Nitrogen-limited chemostats provide the ability to control culture growth rates and provide a basis for studying microorganisms during steady state under defined and constant conditions. By controlling the growth rate of a culture, acclimatization to current conditions is established, allowing for the effects of induced stress (temperature increase) to be interpreted without complication. In observing a time series of LISST PSDs from a culture in which the temperature was raised, distinctions can be drawn between what originally was comprised of only single cells and short chains and what evolved into aggregates of cells and chains. This will enable the investigation of the role of TEP in diatom aggregation.

2. METHODS

2.1 Diatom selection

Several diatom taxa were selected and obtained from the Provasoli-Guillard National Center for Culture of Marine Phytoplankton (CCMP) based on contrasting factors such as size, shape, and whether they are solitary or form chains (see Table 1).

Table 1. Diatoms obtained from the Provasoli-Guillard CCMP. Shown are species' approximate size, simplified geometric shape, and the nutrient medium it was grown in. Diatom names were reduced to a moniker according to their genus, species, and strain number in Provasoli-Guillard National Center for Culture of Marine Phytoplankton (CCMP). F/2 and L1 are nutrient supplement recipes added to artificial seawater (Andersen 2005).

Diatom	Shape	Size (l × w)	Nutrient medium	Notes
SM1332 *Skeletonema marinoi*	Cylinder	20µm × 10µm	L1	Chain-forming
CM1316 *Chaetoceros muelleri*	Cylinder	20µm × 5µm	F/2	Spines
TW1051 *Thalassiosira weissflogii*	Cylinder	20µm × 15µm	F/2	Centric-solitary
PT2561 *Phaeodactylum tricornutum*	Two cones	20µm × 5µm	F/2	Pennate
SC2092 *Skeletonema costatum*	Cylinder	20µm × 10µm	L1	Chain-forming
CC1578 *Chaetoceros contortus*	Cylinder	20µm × 5µm	F/2	Spines
OA1796 *Odontella aurita*	Unique	10µm × 20µm	F/2	Chain-forming
CW2513 *Coscinodiscus wailesii*	Cylinder	200µm × 200µm	L1	Centric - solitary
TR1647 *Thalassiosira rotula*	Cylinder	20µm × 15µm	F/2	Chain-forming

When cultures arrived, 1 ml was taken from each 15 ml culture tube and inoculated into 40 ml of autoclaved artificial seawater (Harrison et al. 1980; Berges et al. 2001), L1 or F/2 nutrients, and incubated at 20 °C (14 h light: 10 h dark) to maintain actively growing cultures. Additionally, 5 ml were taken from each culture tube and diluted with 100 ml of 0.2 µm-filtered artificial seawater already in the LISST chamber to establish archival data in case a strain were to change over time or it was not chosen for initial growth experiments. Diatom taxa listed in Table 1 were continuously maintained in batch culture over the course of the experiment.

2.2 Batch culture LISST characterization (Hypothesis 1)

Experimental design. The following cultures were selected for further LISST characterization during different stages of growth in batch culture: *Coscinodiscus wailesii* (CCMP 2513), *Odontella aurita* (CCMP 1796), *Phaeodactylum tricornutum* (CCMP 2561)*, Skeletonema costatum* (CCMP 2092), *Skeletonema marinoi* (CCMP 1332), *Chaetoceros muelleri* (CCMP 1361), *Thalassiosira rotula* (CCMP 1647), and *Thalassiosira weissflogii* (CCMP 1051). Each diatom was grown in triplicate 1 liter flasks of 500 ml artificial seawater (Harrison et al. 1980; Berges et al. 2001) in L1 (purchased from Provasoli-Guillard CCMP) nutrients at 20 °C (14h light:10 h dark) using sterile technique. It was assumed that cultures were not axenic. While cell counts were taken almost every 24 h, three main sample times were targeted to observe growing concentrations of cells and assess whether diatom cultures appear differently during stages of growth (i.e. lag phase, growth, stationary). Sampling of each diatom's lag,

growth, and stationary phases took place on day 3, 5, and 11 after inoculation and included the following analyses: cell counts and cell sizing, LISST analysis, total and dissolved carbohydrates (phenol-sulfuric acid method), TEP (colorimetric analysis), and chlorophyll *a*.

Cell counts and sizing. One ml from each replicate per day was placed in a small glass vial and preserved with a drop of Lugol's iodine (Parsons et al. 1984) for use in cell counts. To eliminate preservation effects on cell dimensions (Menden-Deuer et al. 2001), the major and minor axes of 75 individual diatoms or chains were measured (25 from each culture flask) using a 50 µm graticule-calibrated Carl Zeiss Axioplan2 microscope and AxioVision software prior to preservation. Cell count determinations were made using a cell hemocytometer (Hauser Scientific Fuchs-Rosenthal or Sedgwick Rafter for *Coscinodiscus*) for all cultures, counting approximately 400 cells per replicate vial (Andersen 2005).

LISST. The LISST 100X Type C (Sequoia Instruments) is a laser-based, forward-scattering particle size analyzer capable of benchtop or *in situ* sampling. By detecting the angle of light scattering off particles, it can estimate and report their equivalent spherical diameters and the total volume each particle size occupies. The subsequent volume concentration data, separated into 32 logarithmically-spaced bins (2.72-460 µm) were processed using a background scattering file using 0.2 µm-filtered water (UHP water) for latex microspheres or filtered artificial seawater for diatoms as blanks in the Sequoia Scientific LISST software. Background scattering measurements were taken before each new LISST session to assure any background particle data from

UHP or artificial seawater would be subtracted from the particle size distributions (PSD). Data were then plotted as a bar chart of average volume concentrations in each bin with error bars representing the standard deviations of the volume concentration in each size bin and as a spline curve running through average volume concentrations. This offered a visual representation of the peaks and troughs and allowed identification of different diatom taxa. Additionally, particle number (*N*) and surface area (*S*) per bin range (in µm) were calculated from the original volume data according to Seinfeld and Pandis (1997) and plotted as spline curves against the size bins. The number of particles per bin range and surface area of particles per bin range, shown below in Equation 1 and Equation 2, can be defined as the number of particles per cubic centimeter (*N*) or the measure of surface per particle (in μm^2) per cubic centimeter (*S*) divided by the natural log of the bin width (D_p) (in µm).

$$N = \frac{dN}{\ln D_p} \qquad (1)$$

$$S = \frac{dS}{\ln D_p} \qquad (2)$$

LISST sampling. Before diatoms were sampled, National Institute of Standards and Technology (NIST)-traceable 6, 25 and 90 µm diameter polystyrene microspheres were acquired from Duke Scientific to determine the accuracy of the LISST, in terms of how it reported equivalent spherical diameters of particles and how the actual volume concentration of spheres corresponded to the reported volume concentration. Concentrated sphere suspension (0.025 g spheres$\cdot g^{-1}$ water) was added in independent dilutions of 100, 200, 400, 800, 1000, and 1200 µl per 100 ml of UHP water and

sampled in the LISST bench top chamber at a rate of 1 Hz for 100 seconds resulting in varying volume spline curve graphs. Next, dilutions were combined and again analyzed with the LISST to determine whether latex spheres of 6, 25 and 90 µm diameter size bins produced three distinct peaks. After sphere counts were performed using a hemocytometer, volume data observed from using the LISST could be compared to volume data calculated from actual microsphere volume and sphere concentration.

Additionally, a monoculture sample of *C. muelleri* was added to the LISST chamber along with artificial seawater to provide dilutions of 100, 90, 70, 50, 30, 20, 10, 5, and 1% (v/v) which was analyzed with the LISST, and cells were counted and sized using a Spencer Lens Co./AO microscope. The purpose of this experiment was to determine whether there was a positive correlation between the concentration of diatoms in a sample and the volume concentration measured by the LISST.

Lastly, at the 3rd, 5th, and 11th day of each diatom's growth curve, 20 ml from each replicate culture was mixed with 80 ml of 0.2 µm-filtered artificial seawater to avoid light attenuation, and slowly poured into the LISST chamber. One hundred measurements, at a rate of 1 Hz, were automatically recorded using the Sequoia Scientific LISST software.

TEP colorimetric analysis. Two 5 ml aliquots of culture per replicate were filtered using a glass filtration apparatus under low pressure (< 1 in. Hg) onto two 0.4 µm polycarbonate filters. To account for interference in the assay between algal chlorophyll and alcian blue light, two types of filters were prepared, a stained filter and an unstained filter. For the stained filter, 0.5 ml of alcian blue stain (0.02% in 0.06%

acetic acid pH 2.5 (Passow and Alldredge 1995)) was added to first filtration column while 0.5ml of UHP water was added to the second control filtration column, followed by two separate rinses of 1 ml of 0.2 µm-filtered UHP water down each column. TEP concentrations were measured using a colorimetric method where the filters were placed in glass boiling tubes before the addition of 2 ml of 80% sulfuric acid under a fume hood (Passow and Alldredge 1995; Thornton et al. 2007). Tubes were agitated 4-5 times over a period of 2 h, the acid was added to 1 cm light path polypropylene cuvettes (VWR Scientific) and absorbances at 787 nm were read using Shimadzu UV-Mini spectrophotometer.

Gum xanthan is a model exopolymer that has been used previously because of its similarity to TEP in that it dissolves in water and will form small, gel-like particles (Passow and Alldredge 1995). 0.1 g of gum xanthan was added to 100 ml of 0.2 µm filtered artificial seawater and ground with a glass manual tissue grinder for 20 minutes. Serial dilutions of the concentrated gum xanthan were performed to obtain final concentrations of 0, 10, 20, 30, and 40 µg per filter when 6 ml was filtered and stained in duplicate as above. A calibration curve was constructed from their spectrophotometric absorbance at 787 nm. After subtracting the chlorophyll blank absorbance from the algal culture samples, the linear regression from the gum xanthan curve was used to calculate TEP concentration in gum xanthan equivalent units (Passow and Alldredge 1995; Thornton et al. 2007).

Chlorophyll a analysis. A 20 ml aliquot per replicate was filtered down onto a 47 mm GF/C filter and frozen at -20 °C until analysis. Five ml of cold (4 °C) 90%

acetone was combined with the macerated filters in 15 ml centrifuge tubes and left to extract for 24 hours. The tubes were centrifuged at 4000 × *g* for 20 minutes and the absorbance of the supernatant extract was measured in a 1 cm light path glass cuvette using a spectrophotometer at four wavelengths (750, 664, 647, and 630 nm). Chlorophyll concentrations for each sample were calculated in Equation 3 according to Strickland and Parsons (1984) where D_x represents the absorbance at a wavelength (nm), v is the volume of acetone (ml), l is the cuvette light path (cm), and V is the volume of filtered water (liters).

$$\text{Chl}_a\ [\text{mg} \cdot \text{m}^{-3}] = (11.6\ D_{665} - 1.31\ D_{645} - 0.14\ D_{630}) \cdot v \cdot l^{-1} \cdot V^{-1} \quad (3)$$

Phenol-sulfuric acid carbohydrate analysis. From each replicate, a 1.2 ml aliquot was designated for total carbohydrate fractions while an additional 1.2 ml aliquot was centrifuged in microcentrifuge tubes at 5000 × g for 20 minutes. The supernatant was reserved to determine the dissolved fraction and both the total fraction and dissolved fraction were frozen until analysis. A calibration curve was constructed with the addition of 1 g of D-glucose in 1000 ml of UHP water creating replicate dilutions of 100, 50, 40, 30, 20, 10, 5 and 0 µg D-glucose · ml^{-1}. Using the phenol-sulfuric acid method adapted from DuBois et al. (1956), the calibration curve and the total and dissolved fractions were analyzed spectrophotometrically following the combination of 0.8 ml of sample, 0.4 ml phenol, and 2 ml of concentrated sulfuric acid in a glass boiling tube. Concentrations of total and dissolved fractions for each replicate were calculated relative to their absorbance at 485 nm from the calibration curve in µg of D-glucose equivalents per milliliter.

Roller experiment. To properly gauge the usefulness of the LISST as a tool to detect changes in particle size distributions, a roller experiment was set up to induce aggregation in *Skeletonema costatum* cultures. Four identical *S. costatum* cultures were grown in 1 L borosilicate flasks with 500 mL of autoclaved artificial seawater and sterile L1 nutrients. After 15 days 150 ml of each culture was distributed amongst to each of 12 identical 200 ml polyethylene dark bottles (VWR Scientific). One set of four bottles were set aside and incubated at 20°Cto be sampled with the LISST without rolling. The other set of the three sets of four bottles were each placed upon a rolling platform and rolled at approximately 12 rpm and incubated separately at temperatures of 20, 25 and 30°C. After four hours the cultures are removed from the incubation chamber were sampled with the LISST. Spline curves of the volume normalized particle size distributions were graphed using the mean ± SD (n = 4). No other measurements were taken as this experiment was only being used to gauge the LISST's ability to detect aggregation through changes in each temperatures PSD.

2.3 Temperature and growth rate alteration of a chemostat (Hypothesis 2)

Chemostat construction. Unlike an initially nutrient-replete batch culture where conditions change constantly throughout its use, chemostat cultures allow for steady and constant growth conditions using nitrate limitation. In a chemostat, as new medium is added, an equivalent volume of cell culture is automatically removed from the vessel, adding only the new medium and nutrients required for the maintenance of biomass and, therefore, providing a steady supply of culture under constant physiological conditions. Growth rate of the culture is defined through Equation 4 (Andersen 2005): where μ is

the specific growth rate of the population, F is the medium flow rate (liters·hour^{-1}), and V is the volume of the culture vessel (liters), all equal to D the dilution rate.

$$\mu = \frac{F}{V} = D \qquad (4)$$

In the laboratory environment a chemostat removes the stresses of changing conditions like light and dynamic concentrations of multiple nutrients, allowing for the effects of induced stress from temperature change to be closely monitored. A chemostat culture system was constructed as in Figure 3. Two liter, borosilicate cultures bottles (VWR Scientific), when inoculated, were sealed with silicone rubber bungs and placed in a temperature-controlled water bath in a glass aquarium (VWR recirculating pump model 1196D). Sealed inside each bottle was a magnetic stir bar which would be turned by magnetic stir plates below each culture bottle located underneath the aquarium. Two fluorescent light banks (40 watt Philips Daylight Deluxe bulbs) were placed against either side of a glass aquarium, supplying 70-80 µmol photon (Li-Cor directional photometer) surface luminance to either side of the cultures. Air supply, provided by two aquarium air pumps, was air-stone bubbled through autoclaved reverse osmosis water and through two 0.2 µm air filters (Pall) before being distributed to each culture bottle through the polyurethane bung with 3/32" silicon rubber tubing (Tygon). Fresh medium and nutrients (according to Table 2) were provided through through the silicone rubber bungs from a sterile 20 l polycarbonate carboy (VWR Scientific) using a peristaltic pump at 6.75 rpm (Watson-Marlow) using 1.3mm internal diameter manifold tubing (FisherBrand) and a network of 3/32" silicon rubber tubing (Tygon). Because culture bottles were under a slight positive pressure, effluent waste was expelled through

borosilicate glass pipettes set at the height of 1 l inside the bottles into a VWR Scientific plastic carboy containing bleach to kill microorganisms present in the waste.

Preparation of axenic batch cultures used to inoculate the chemostats. Several failed attempts were made to grow both *C. muelleri* and *S. costatum* under nitrate limitation using 25 µm $NaNO_3$. *C. muelleri* was grown successfully with 50 µm $NaNO_3$ (final concentration), providing a level of biomass needed for proper maintenance of steady state and sufficient biomass for the experiments.

All glassware was autoclave sterilized and all liquids were filter sterilized through a 0.2 µm filter. A set of two 2000 ml sealable borosilicate bottles, each containing 1200 ml of artificial seawater, were sterilized and nutrients were added according to Berges et al. (2001), with the exception of $NaNO_3$ (100 µM N), KH_2PO_4 (50 µM P), and $Na_2SiO_3•_9H_2O$ (100 µM Si), along with a 20 ml inoculate of a healthy *Chaetoceros muelleri* (CCMP 1316) culture. After cultures were incubated for 2 days at 20 °C (14 h light: 10 h dark), penicillin G (final concentration 400 $\mu g \cdot ml^{-1}$) and ampicillin (200 $\mu g \cdot ml^{-1}$) were added, with streptomycin (200 $\mu g \cdot ml^{-1}$) added 24 h later. To limit total exposure to antibiotics to 48 hours, two additional autoclaved borosilicate bottles containing 1000 ml of artificial seawater, were combined with the two bottles containing culture, halving antibiotics, nutrients, and biomass.

The diluted *C. muelleri* cultures were distributed equally (600 ml each) among four 2000 ml bottles, containing nutrients in final concentrations listed in Table 2 and placed into the water bath and aseptically connected to the chemostat system to await the start of the dilution 48 hours later.

Chemostat dilution and temperature manipulation. In order to properly test the effects of temperature on a steady-state culture while minimizing the effects of prokaryote interference in carbon production and consumption, the set of 4 cultures of *C. muelleri* were grown and held in steady-state using nitrogen limitation (50 µM $NaNO_3$ final concentration) in chemostats (see Fig. 3 for setup) under constant light and at a temperature of 20 °C. N limitation was verified through bioassays at each temperature change by removing 40 ml from each culture bottle into three sets of four plastic culture flasks, spiking four with 100 µM $NaNO_3$, four with nutrients (according to Table 2) without nitrogen, and four with no nutrient addition as a control. Cell counts were taken before incubation with nutrients and after a 48 h incubation with nutrients.

Table 2. Chemostat nutrient medium. Nutrient supplement and artificial seawater final concentrations adapted from Harrison et al. (1980) and Berges et al. (2001).

Nutrient supplements		Artificial seawater	
Major nutrient I—nitrate	Final conc.	Anhydrous salts	Final conc.
$NaNO_3$	50 μM	NaCl	363 mM
Major nutrient II—phosphate		Na2SO4	25.0 mM
$NaH_2PO_4 \cdot H_2O$	50 μM	KCl	8.04 mM
Major nutrient III—silicate		$NaHCO_3$	2.07 mM
$Na_2SiO_3 \cdot 9H_2O$	100 μM	KBr	725 μM
Metals stock I—iron		NaF	323 μM
$FeCl_3 \cdot 6H_2O$	6.56 μM	Hydrated salts	
$Na_2EDTA \cdot 2H_2O$	6.56 μM	$MgCl_2 \cdot 6H_2O$	41.2 mM
Metals stock II—trace metals		$CaCl2 \cdot 2H_2O$	9.14 mM
$ZnSO_4 \cdot 7H_2O$	254 nM	$SrCl2 \cdot 6H_2O$	82 μM
$CoSO_4 \cdot 7H_2O$	5.69 nM		
$MnSO_4 \cdot 4H_2O$	2.42 μM		
$Na_2MoO_4 \cdot 2H_2O$	6.1 nM		
Na_2SeO_3	1 nM		
$NiCl_2 \cdot 6H_2O$	6.3 nM		
$Na_2EDTA \cdot 2H_2O$	8.29 μM		
Vitamin stock			
Thiamine-HCl	297 nM		
Biotin	4.09 nM		
B12	1.47 nM		

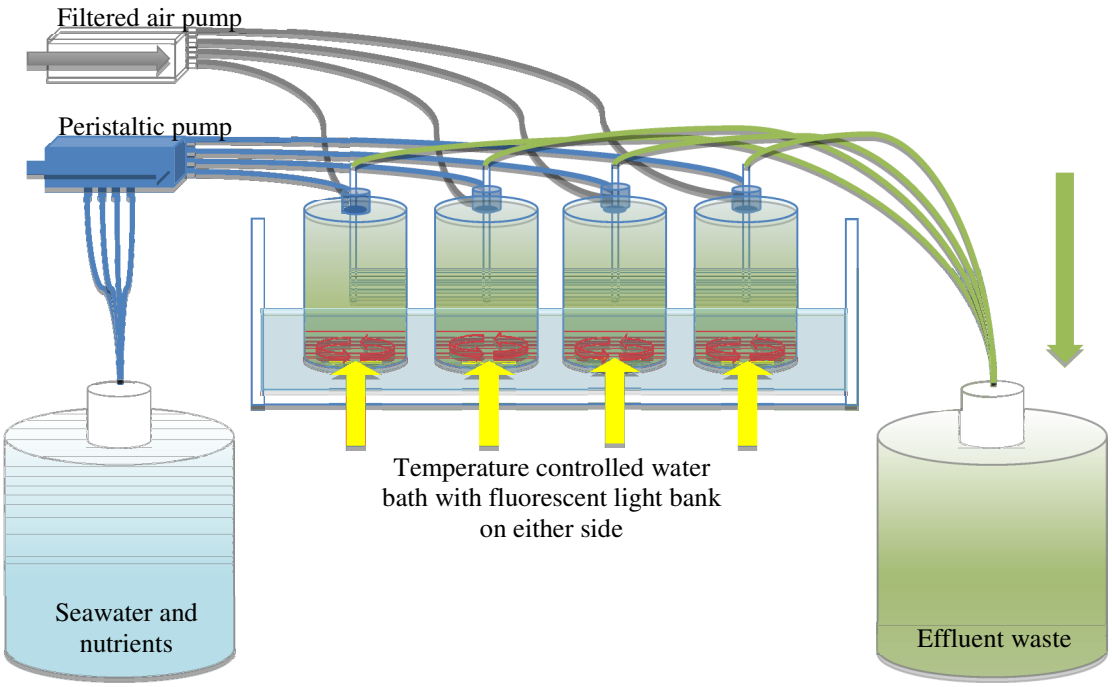

Fig. 3. Chemostat simplified diagram and setup photograph. Photograph depicts four chemostat culture vessels inside the aquarium water bath with light banks on either side. Vessels were sealed initially and before nutrient and air lines were connected.

First, while under a dilution of $0.6 \cdot d^{-1}$and temperature at 20 °C and measurements were taken according to the methods used previously (with the exception of TEP - See *Image Analysis* methods) to obtain data about the LISST PSD, total carbohydrates, TEP, chlorophyll, and cell counts. Subsequent measurements were taken on both the first, third, and fifth days following the start of the dilution. Then, temperature in the cultures were raised at a rate of no more than 1 °C per hour, from 20 °C to 22.5 °C, allowing for 5 days for acclimatization. Measurements were repeated on the first, third and fifth days for each temperature change thereafter, 22.5 °C to 27 °C, then 27 °C to 20 °C. Total duration of the experiment was 48 days.

TEP – image analysis. To provide a more quantitative measurement of the TEP present, real particle numbers and real particle areas were computed using image analysis rather than a colorimetric comparison against a TEP proxy (gum xanthan) (Logan et al. 1994). One ml from each replicate chemostat culture was filtered onto a 0.4 µm pore size white polycarbonate filter and stained as in the TEP colorimetric method above, however the filter was then mounted in fluorescent stable microscopy oil atop a GE Osmotics CytoClear® frosted slide and observed underneath 100x brightfield and using a Carl-Zeiss Axioplan2 microscope. Using the identical exposure and light intensity settings, ten adjacent images were taken moving from the right to left on each stained slide. The National Institutes of Health's (NIH) ImageJ open source image analysis suite was used to identify and size TEP particles present. The TEP particles in the images were identified by their dark contrast relative to the background by thresholding them using the "triangle" algorithm developed for chromosome counting

and analysis (Zack et al. 1977). The suites' "Analyze particle" algorithm was used to draw a perimeter around each individual particle, recording particle areas as small 0.412 μm^2 (one pixel) with no upper limit to particle area.

Quality control. To ensure that cultures were nitrogen limited, 20 ml samples from each of the four cultures and from the carboy containing fresh medium were filtered through a 0.2 μm syringe filter (Nalgene) and frozen in plastic scintillation vials for autoanalysis of nitrite, nitrate, urea, phosphate, and silicate at the Geochemical & Environmental Research Group, Texas A&M University (GERG).

Temperature of the chemostat water system was set and adjusted using a NIST-traceable mercury thermometer (VWR Scientific) while temperature of the individual culture vessels were recorded using a calibrated electronic thermometer (VWR Scientific). Temperature in the water bath from inlet to outlet varied less than 0.1 °C and temperatures inside each culture vessel varied less than 0.1 °C when compared to the water bath temperature.

After chemostat had been running for 14 days, dilution rate was checked by collecting the effluent waste from each culture vessel over a period of 24 hours and calculating dilution from each measured volume. Dilution rates between flasks varied less than 0.03 d^{-1} and the measured dilution rate varied from the theoretical rate of 0.6 d^{-1} by 0.05 d^{-1}.

3. RESULTS

3.1 Polystyrene microsphere LISST measurements

Independent LISST measurements of the 6 µm, 25 µm and 90 µm polystyrene microspheres yielded particle size distributions (PSD) each featuring a single peak with a maximum volume fraction corresponding to each particles diameter. Fig. 4a, Fig. 4b, and Fig. 4c represent these PSD where the points along each curve represent the mean fraction of the total volume concentration in each size bin (n = 300). The LISST instrument sizes and categorizes particle diameters using a logarithmically-spaced scale from 2.5 to 500 µm but I report all size bins as the median values for each bin range. Therefore, the 6, 25, and 90 µm particle distributions were not allotted to a single size bin but rather a range of size bins. The 90 µm and 6 µm microspheres (Fig. 4c and Fig. 4a) are represented by a central peak at the 87.9 um size bin with secondary peaks at the 74.5 and 104 µm bins and by a central peak at 7.33 µm with secondary peaks at 6.21 and 8.65 µm, respectively. The 25 µm microspheres (Fig. 4b) are also shown with a central peak but shared between the 23.4 and 27.6 µm bins along with secondary peaks on either side. While the single, but broad, peaks in all three graphs (Fig. 4a, Fig. 4b, Fig. 4c) can be explained by the manner in which the LISST measures particles, large volume concentrations at the 2.72 and 460 µm are also evident. Although UHP water was used to dilute the microspheres and the LISST chamber was cleaned thoroughly, it is reasonable to assume that dust or other particles could explain the detection. Particles

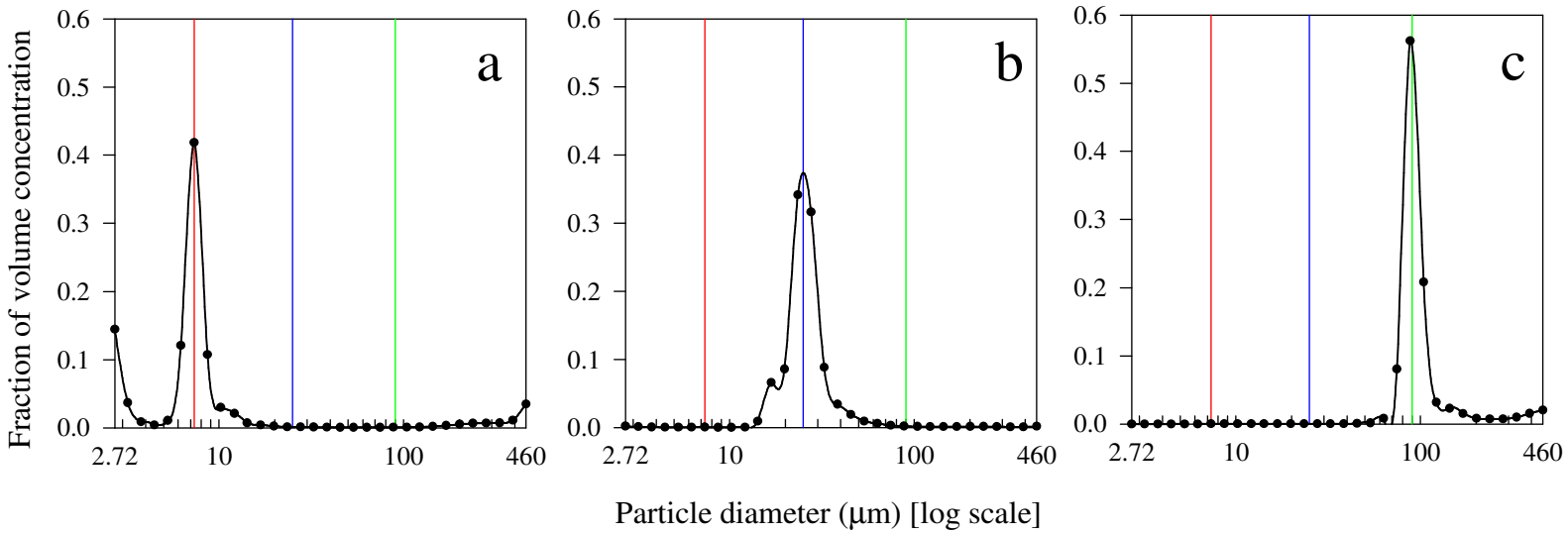

Fig. 4. Particle size distribution (PSD) of polystyrene microspheres in 32 size bins normalized to the total volume concentration of particles. Curves drawn through the mean proportion of volume concentration (black circles) in each size bin (n = 100). (a), 6 µm diameter microspheres. Red reference line indicates 6 µm (b), 25 µm diameter microspheres. Blue reference line indicates 25 µm (c), 90 µm diameter microspheres. Green reference line indicates 90 µm.

detected smaller than 2.5 µm and larger than 500 µm are placed into either the 2.72 or 460 µm size bin at either end of the bin range, inflating the volume concentrations for those bins. While this could cause false detection and misrepresentation of volume concentrations, integrating volume concentrations across all size bins from multiple runs at different concentrations of 25 µm beads resulted in a significant linear relationship ($r^2 = 0.98$; CI 95%) between bead concentration (µl beads per 100 ml water) and LISST-detected volumes (Fig. 5). This not a one-to-one relationship, however, LISST volume measurements underestimate actual particle volume by a factor of 10. It is unclear why the LISST does not accurately detect total volume concentrations but it has been speculated this is an error in how the LISST algorithm categorizes particle ranges (Agrawal et al. 2008).

3.2 Diatom LISST measurements

Diatom sampling attempted to target each diatom during separate phases in batch cultures: growth, lag, and stationary phases. A visual inspection of each species' culture flasks was used as the indicator to target these phases. Fig. 6, Fig. 7, Fig. 8,Fig. 9, Fig. 10 and Fig. 11 indicate when cell counts were taken (mean ± SD; n = 3) and when measurements were taken for the LISST, total carbohydrates (mean ± SD; n = 3) and chlorophyll *a* (mean ± SD; n = 3). Except in the case of *Skeletonema marinoi* where total carbohydrate analysis failed, each diatom species showed an exponential increase in cell concentration from 0-50 hours after inoculation, reaching a maximum biomass of around 1×10^6 cells $\cdot$ ml^{-1} except in the case of *Coscinodiscus wailesii* (100 cells $\cdot$ ml^{-1})

and *Phaeodactylum tricornutum* (5×10^6 cells $\cdot$ ml^{-1}). Additionally, as biomass increased in all cultures, both chlorophyll and total carbohydrates saw increases of 10 µg $\cdot$ l^{-1} and 10 µg $\cdot$ ml^{-1}, respectively. However, after the first sampling day, changes in carbohydrates and chlorophyll vary with each diatom likely due to the time difference between sample days 2 and 3. To show that diatom PSDs vary little during batch culture growth, PSDs for *Chaetoceros muelleri* in Fig. 12 (and Appendix I) depict how the general shape of PSD peaks do not change position or height during the three sample days. However, mean PSDs throughout the entire growth curve for each diatom can be seen in Fig. 13 and Fig. 14. Because diatom biomass differed between species and between sampling times, LISST particle size distributions (PSD) were normalized independently for each species according to the fraction of the total volume each size bin occupied. These normalized LISST PSD are visualized in Fig. 13 and Fig. 14, where the points along each curve represent the mean fraction of the total volume concentration in each size bin (n = 900).

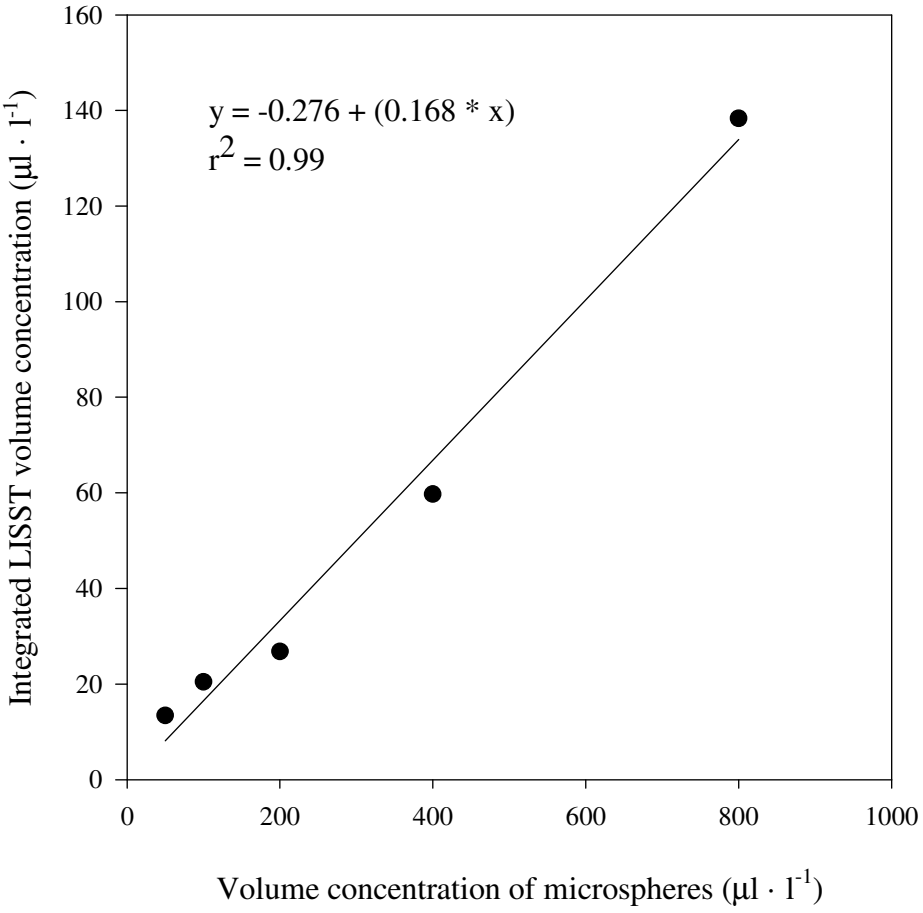

Fig. 5. Relationship between 25 µm diameter bead suspension (2.5% w/v) and integrated LISST volume.

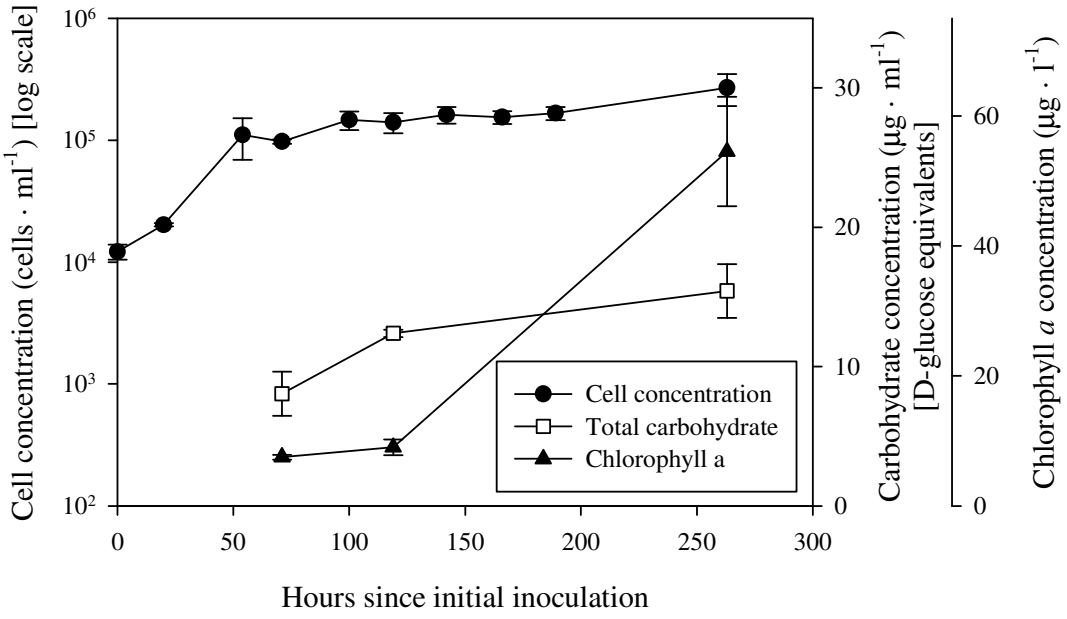

Fig. 6. Growth curve of *Thalassiosira weissflogii*. Solid circles represent cell concentration (mean ± SD; n = 3). Open squares and closed triangles represent total carbohydrates and chlorophyll *a* concentration, respectively (mean ± SD; n = 3).

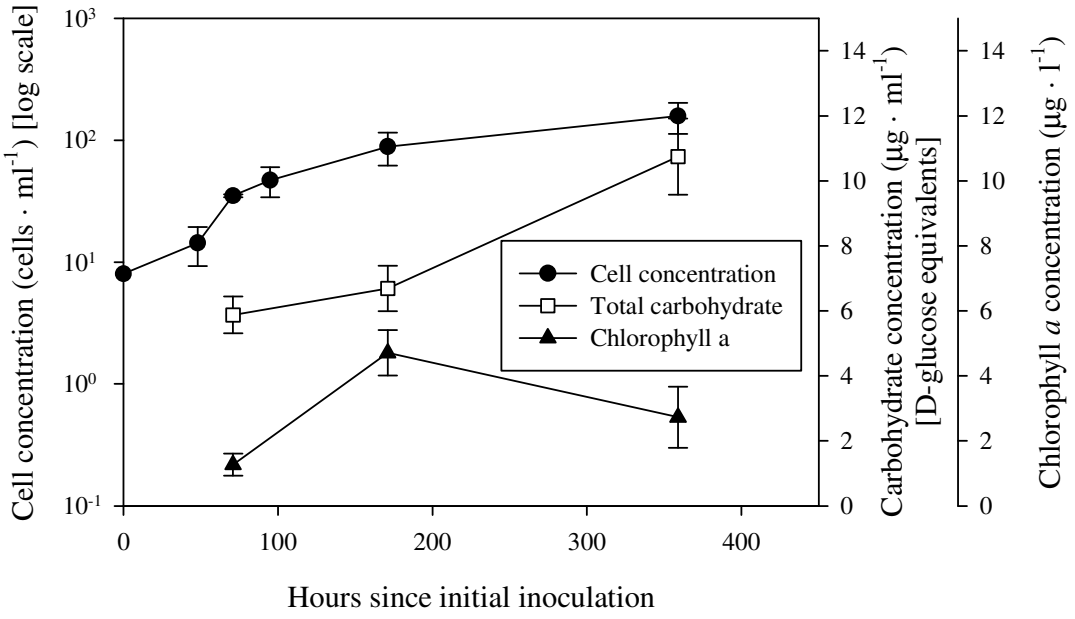

Fig. 7. Growth curve of *Coscinodiscus wailesii*. Solid circles represent cell concentration (mean ± SD; n = 3). Open squares and closed triangles represent total carbohydrates and chlorophyll *a* concentration, respectively (mean ± SD; n = 3).

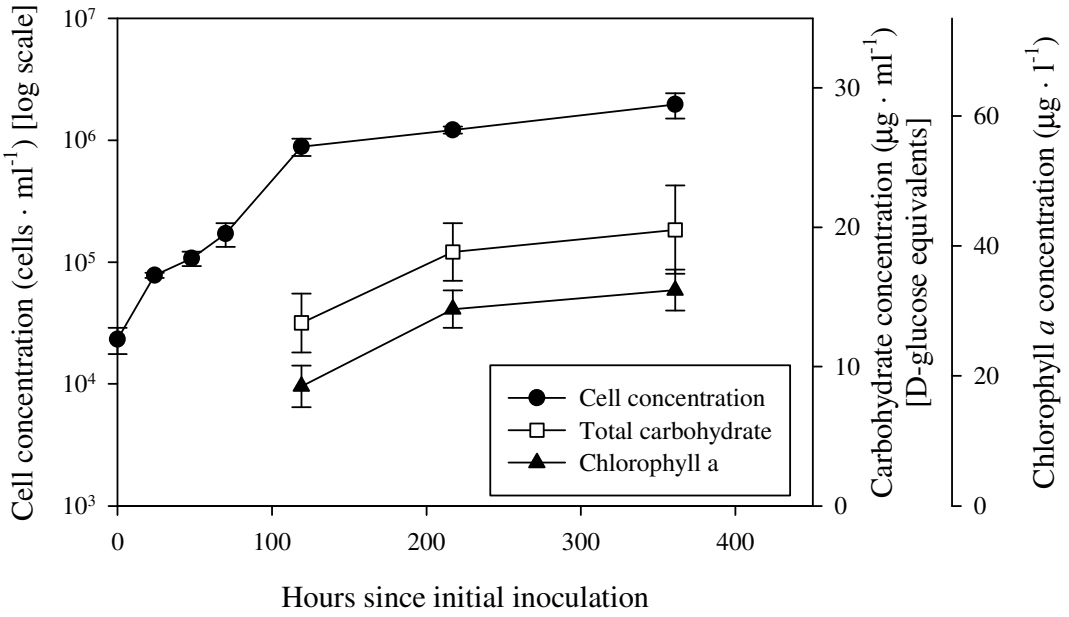

Fig. 8. Growth curve of *Chaetoceros muelleri*. Solid circles represent cell concentration (mean ± SD; n = 3). Open squares and closed triangles represent total carbohydrates and chlorophyll *a* concentration, respectively (mean ± SD; n = 3).

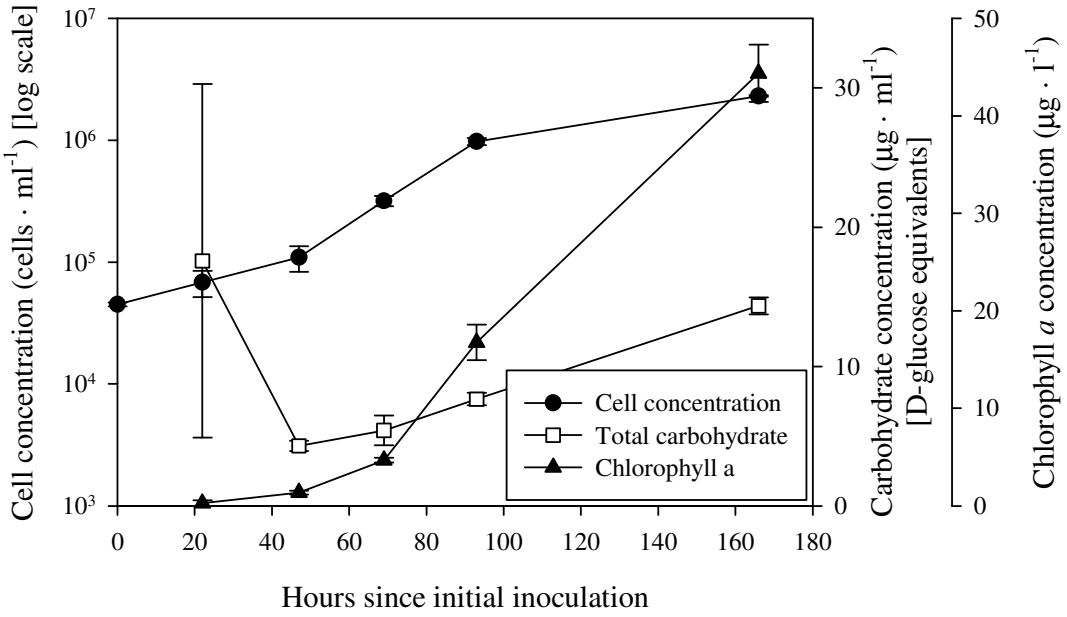

Fig. 9. Growth curve of *Phaeodactylum tricornutum*. Solid circles represent cell concentration (mean ± SD; n = 3). Open squares and closed triangles represent total carbohydrates and chlorophyll *a* concentration, respectively (mean ± SD; n = 3).

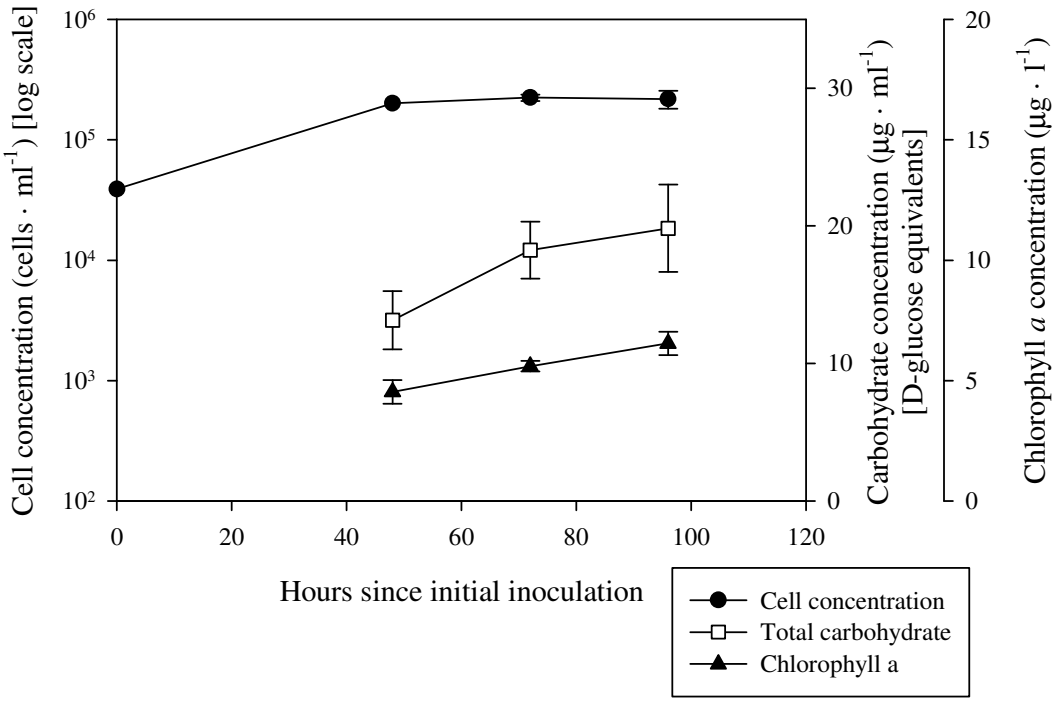

Fig. 10. Growth curve of *Skeletonema costatum*. Solid circles represent cell concentration (mean ± SD; n = 3). Open squares and closed triangles represent total carbohydrates and chlorophyll *a* concentration, respectively (mean ± SD; n = 3).

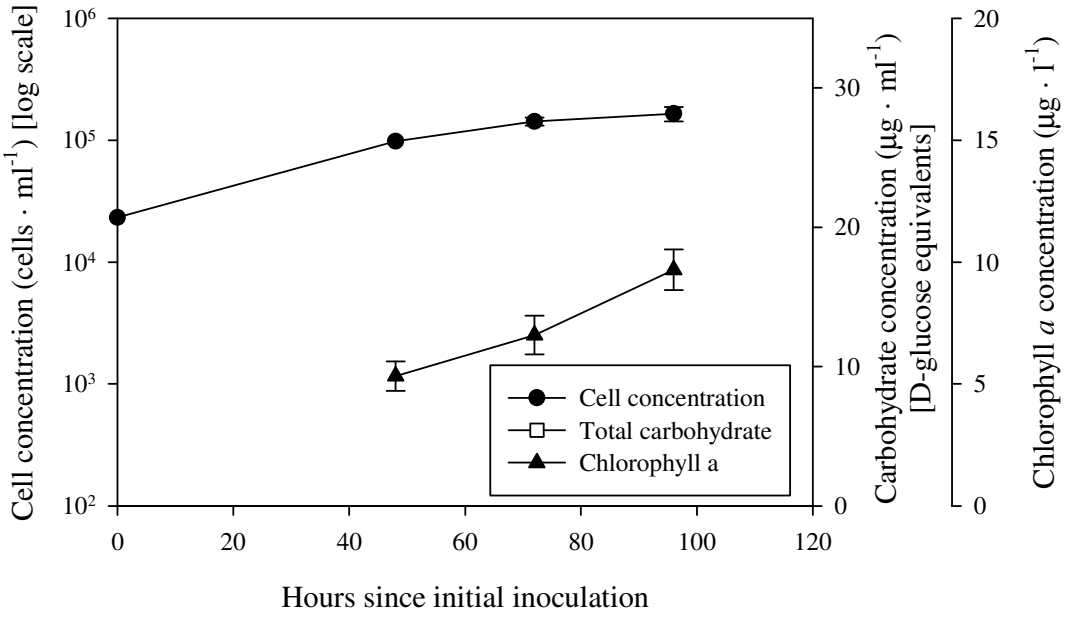

Fig. 11. Growth curve of *Skeletonema marinoi*. Solid circles represent cell concentration (mean ± SD; n = 3). Open squares and closed triangles represent total carbohydrates and chlorophyll *a* concentration, respectively (mean ± SD; n = 3). Total carbohydrate data was not recorded.

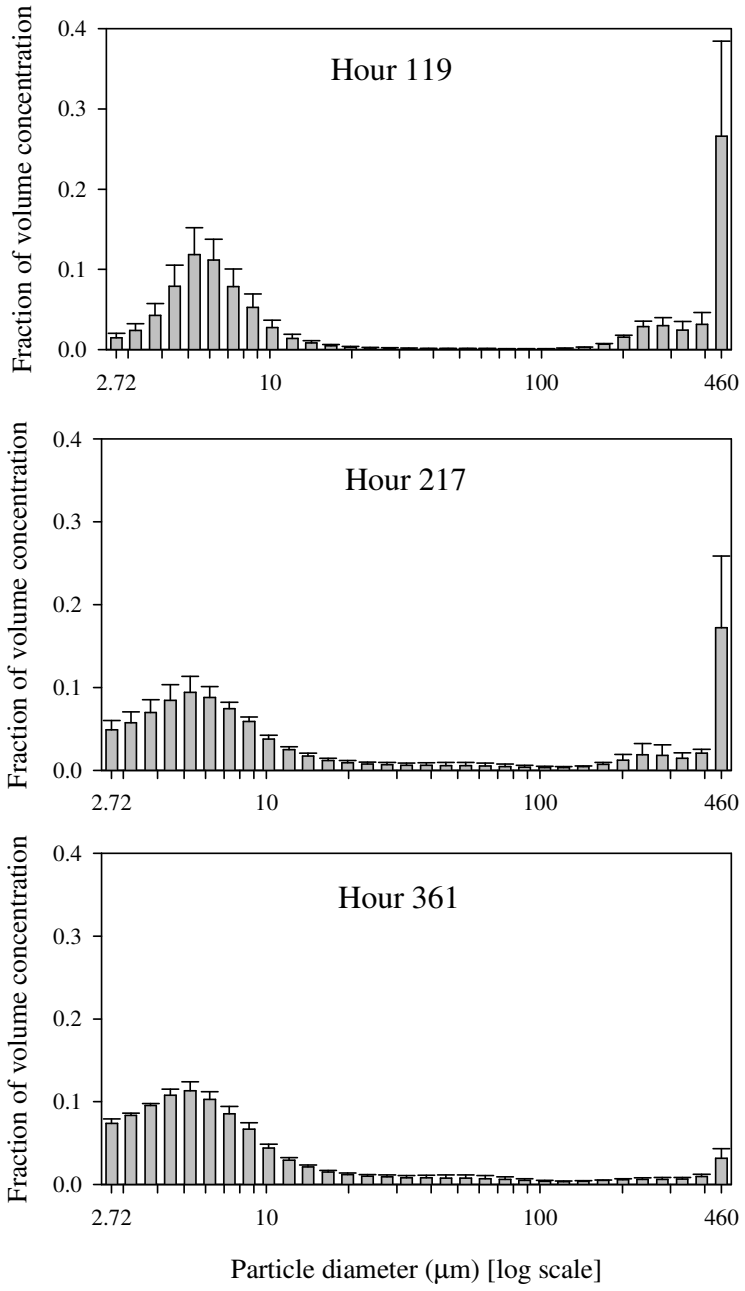

Fig. 12. Particle size distribution (PSD) of *Chaetoceros muelleri* during batch culture experiment. Panels represent the PSDs for sample days 1, 2, and 3. Bars represent the fraction of total volume concentration (mean + SD; n = 3). See Fig. 8 for growth curve.

Light green and dark green highlighted regions behind each curve represent the ranges of minor and major (width and length) axis cell dimensions, respectively, measured under a microscope at 400x magnification (n = 75). Lengths, widths, and cell volumes calculated from mean cell dimensions using a geometric shape are available for each species in Table 3 (n = 75).

Table 3. Measured diatom dimensions, simplified geometric shapes, simplified geometric volumes per cell and calculated volume per cell based on LISST peaks. 25 cells from each culture flask were measured at 400x magnification and pooled together for 75 total measurements per diatom.

Diatom	Geometric Shape	Length × Width ±STDEV	Geometric Volume	LISST spectra peaks Length × Width	Volume from LISST peaks
T. weissflogii	Cylinder	13.9 ±2.92 µm × 7.68 ±1.01 µm	644 μm^3	7.33 µm	309.31 μm^3
S. costatum	Cylinder	28.5 ±12.2 µm × 5.83 ±1.14 µm	760 μm^3	63.1 × 5.27 µm	1376.38 μm^3
S. marinoi	Cylinder	16.9 ±47.4 µm × 7.29 ±1.83 µm	704.8 μm^3	63.1 × 5.27 µm	1376.38 μm^3
P. tricornutum	Two cones	16.3 ±8.07 µm × 4.8 ±1.19 µm	98.2 μm^3	8.65 × 2.72 µm	50.26 μm^3
C. wailesii	Cylinder	221 ±11.2 µm × 189 ±12.4 µm	7.23×10^6 μm^3	237 µm	1.04×10^7 μm^3
C. muelleri	Cylinder	7.37 ±1.02 µm × 5.91 ±0.87 µm	201.9 μm^3	7.33 µm	309.31 μm^3

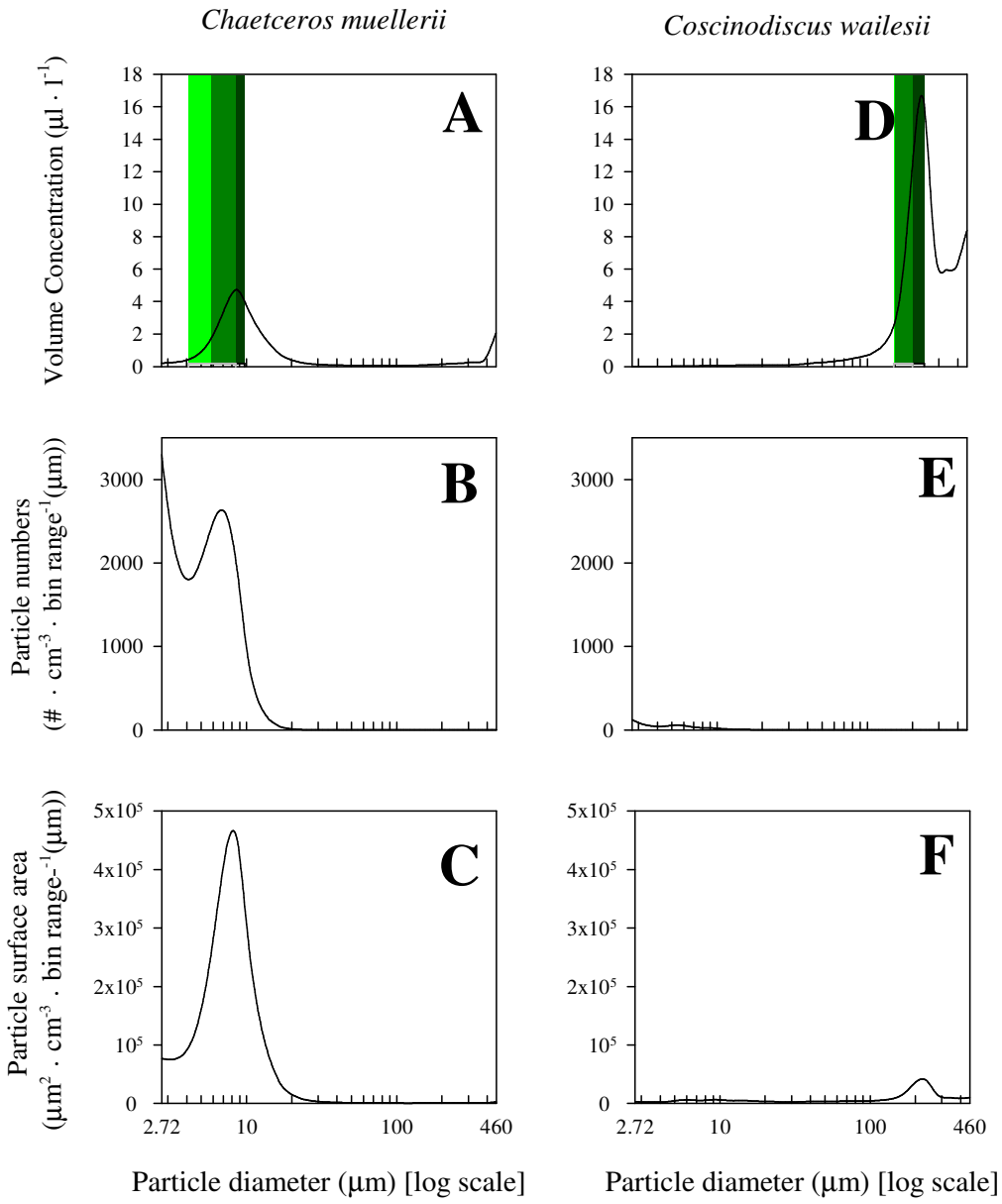

Fig. 13. Particle size distributions (PSD) of two diatom species in 32 size bins. Curves drawn through the mean proportion of volume concentration in each size bin (n = 900). Light green and dark green shaded regions represent the ranges of cell widths and lengths measured under a microscope at 400x magnification. (a), Volume concentration as measured by the LISST (b), Volume concentration in each size bin divided by spherical volume per particle (c). Volume concentration in each size bin divided by spherical surface area.

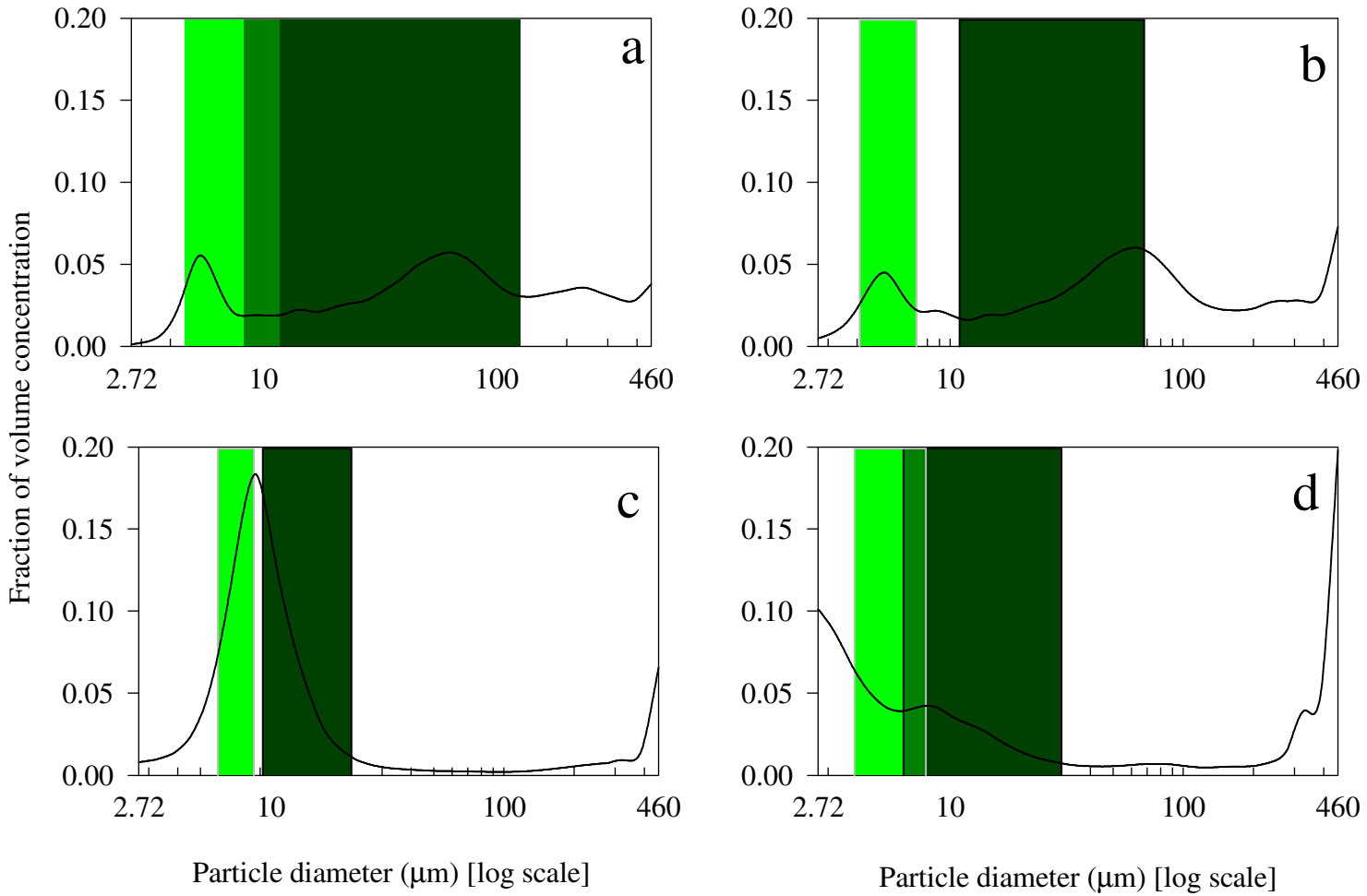

Fig. 14. Particle size distributions (PSD) of four diatom species in 32 size bins normalized to the total volume concentration of particles. Curves drawn through the mean proportion of volume concentration in each size bin (n = 900). Light green and dark green shaded regions represent the ranges of cell widths and lengths measured under a microscope at 400x magnification. (a) *Skeletonema marinoi* (b) *Skeletonema costatum* (c) *Thalassiosira weissflogii* (d) *Phaeodactylum tricornutum.*

Additionally, *S. costatum* and *S. muelleri* are chain-forming diatoms, therefore lengths were reported in the manner the LISST would detect them: as total chain length with number of cells per chain, instead of individual cell length. Fig. 15 features histograms showing the distribution of number of cells per chain (n = 225) for both *S. costatum* and *S. muelleri*, respectively. *S. costatum* chains were not distributed normally and ranged from 1 to 6 cells per chain with the highest chains skewed left with over 130 chains. *S. marinoi* also featured a non-normal distribution with a wider range of 1 to 14 cells per chain, 2-6 cells per chain having the highest distribution.

While the highlighted regions overlap where each diatom PSD peaks, the size of these regions illustrates the variation in cell length, width, and chain length (in the case of *S. costatum* and *S. muelleri*). *Chaetoceros muelleri*, *Coscinodiscus wailesii,* and *T. weissflogii* (Fig. 13a, Fig. 13a, Fig. 14c) individual cells have little variation between length and width (Table 3), resulting in PSD with a single, broad peak, indicating detection of both the major and minor axes of a cell. The *P. tricornutum* (Fig. 14d) PSD shows two overlapping peaks corresponding to the lengths and widths measured in individual cells centered at 2.72 and 7.33 µm. *S. costatum* and *S. marinoi* (Fig. 13b and Fig. 13c), two closely-related species, exhibit PSD that, while overlapping in many peak locations, vary in both peak width and relative volume concentration.

Fig. 13 represents the volume concentrations and particle size distributions across size bins in terms of number of volume concentration, particles present per bin, and surface area of particles per bin for each diatom. When comparing the volume concentration, particle number, and surface area plots between *Coscinodiscus wailesii*

and *Chaetoceros muelleri*, obvious trends in how each diatoms cell dimensions and cell concentration affect its PSD. In terms of volume both comprise a single peak, *C. wailesii* dominating the large size bins while *C. muelleri* dominates the small. However, *C. wailesii* cells are very large so particle numbers were low, 10 cells $\cdot$ ml^{-1}, in comparison to *C. muelleri* particle numbers, upwards of 3.5 x 10^4 cells $\cdot$ ml^{-1}. Additionally, *C. muelleri* surface area also dominates when compared to *C. wailesii*, despite the large difference in cell size between species. These are expected results when comparing the high surface area to volume difference between *C. wailesii* and *C. muelleri*.

A feature present across all the diatom PSDs is particle detection at both the smallest (2.72 µm) and largest (460 µm) size bins. This feature is very evident in the all the figures presented graphs for *P. tricornutum*, *Skeletonema costatum* and *Skeletonema marinoi, Coscinodiscus wailesii, and Chaetoceros muelleri* (Fig. 13 and Fig. 14). Particle detection between major peaks can be explained by variation in single cell dimensions and also by long cell chains or cell aggregates.

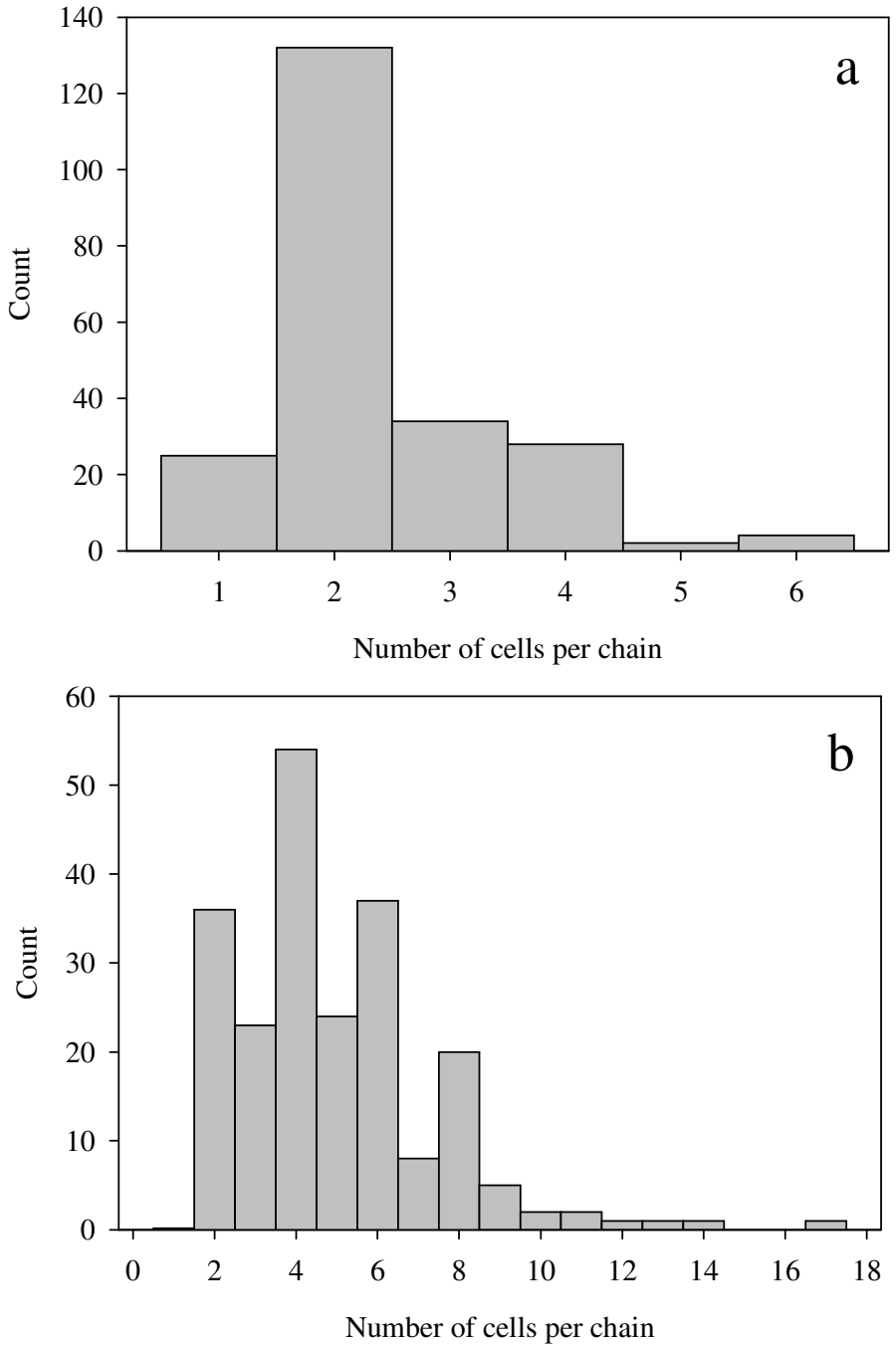

Fig. 15. Distribution of cell chain length (cells per chain) in two chain-forming diatom species (a) Distribution of *Skeletonema costatum* chain length (n = 225) (b) Distribution of *Skeletonema marinoi* chain length (n = 225).

However, particle detection in the 2.72 or 460 µm bin did not correspond to the detection of a single cell or a cell chain and could only result from cell fragments or prokaryote cells and large aggregates, respectively.

3.3 *Chaetoceros muelleri* dilution series

Fig. 16 shows the relationship between diatom biomass determined from cell counts and integrated volume concentration using the LISST. Laser light was attenuated significantly when cell concentrations reached 8 x 10^5 cells · ml^{-1}, causing estimated volume concentration to decrease sharply. In this monoculture situation, careful dilutions of a culture demonstrates that total LISST volume and cell concentration have a proportional, linear relationship ($r^2 = 0.92$).

3.4 *Skeletonema costatum* aggregation

Equal volumes of *S. costatum* were gently rolled at 20, 25, and 30°C and sampled with the LISST to generate particle size distributions (PSD), showing the effect of temperature change on aggregate formation in a diatom batch culture. For comparison, an unrolled volume of *S. costatum* also sampled with the LISST. Fig. 17 illustrates the volume normalized PSDs for each treatment.

Although these *S. costatum* cultures were taken from cultures used to generate Fig. 13b 3 months earlier than this experiment, the unrolled 20°C PSD in Fig. 17a closely resembles the original PSD shown in Fig. 13b. Even upon rolling the culture with no temperature change, Fig. 17b immediately differed from the baseline set in Fig. 17a showing an increase in volume concentration of large particles (aggregates) and disappearance of volume in the size bins representing single cells. The peak centered

around 3-5 µm lowered by 5% while the large size bins, centered around 150 µm, increase by 5%. Rolling the culture at 25°C exhibits a similar pattern as rolling at 20°C but with less overall change in size bins. Rolling the culture at 30°C results in the same pattern: decreasing concentration amongst the small size bins and a large increase in concentration at the large size bins but with even further increase at the two largest size bins, 390 and 460 µm. When comparing each treatment (unrolled at 20°C and rolled at 20, 25, and 30°C), there is a statistically significant difference between treatments ($F_{3,31} = 3.29$, $p = 0.024$) but no significant difference between size bins at each treatment ($F_{3,31} = 1.06$, $p = 0.40$).

3.4 Chemostat culture experiment

Fig. 18 shows the cell concentration with time, from day 1 when dilution was started until day 48 at the end of the experiment. Initially, because of the tiny variance between cell concentration on days 3, 4, and 5, biomass was assumed to be in steady state, so sampling began and continued until day 17 when the temperature was raised to 22.5°C. Biomass continued to increase and the chemostat system biomass came to a steady state as mean cell concentration was $6.9 \times 10^5 \pm 6\%$ cells $\cdot$ ml^{-1} between days 25 and 48 (Fig. 18 and Fig. 19). Correlation values in Table 4 indicate there is no significant correlation between cell counts and temperature ($p < 0.05$).

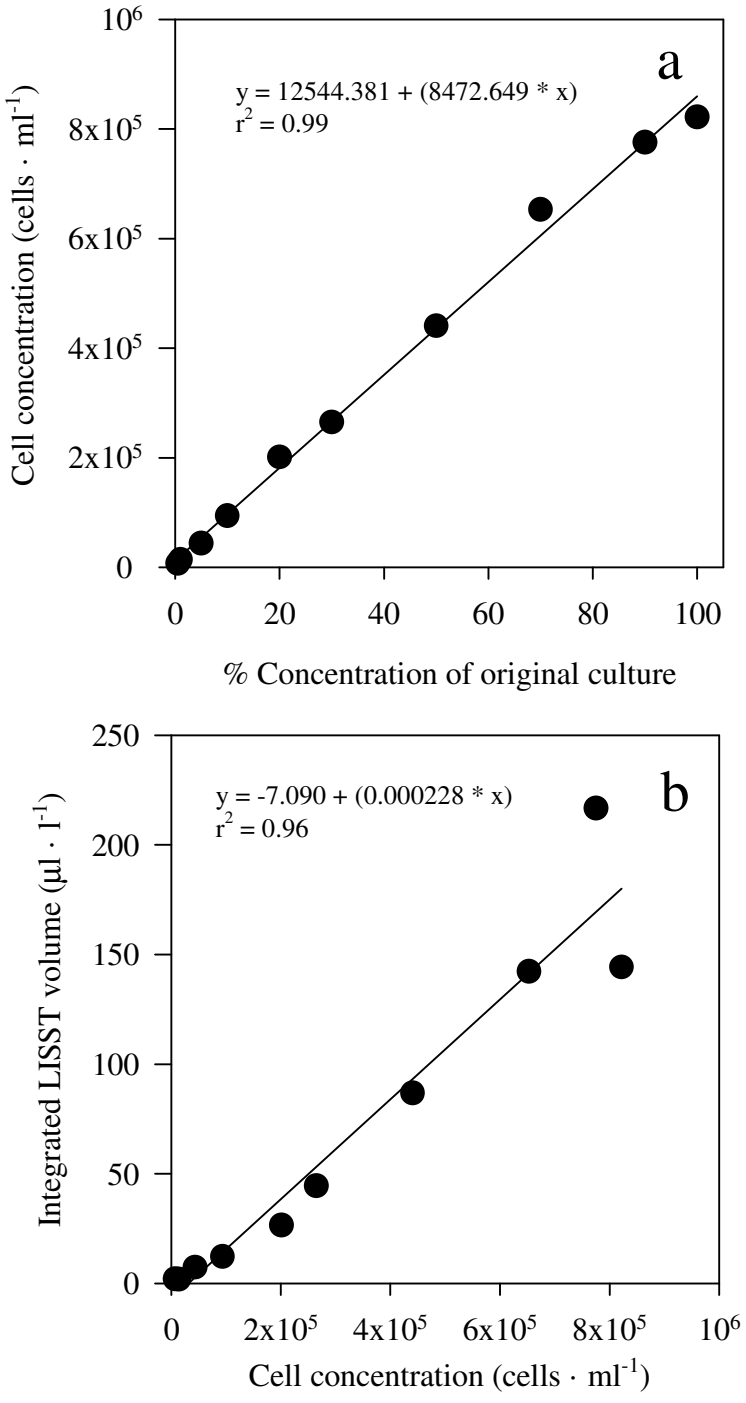

Fig. 16. *Chaeotoceros muelleri* dilution series compared to integrated LISST particle size distribution (PSD) volumes. (a), Relationship between cell concentration and dilution of original culture ($r^2 = 0.99$) (b). Relationship between cell concentration and integrated LISST volume (n = 100) ($r^2 = 0.96$).

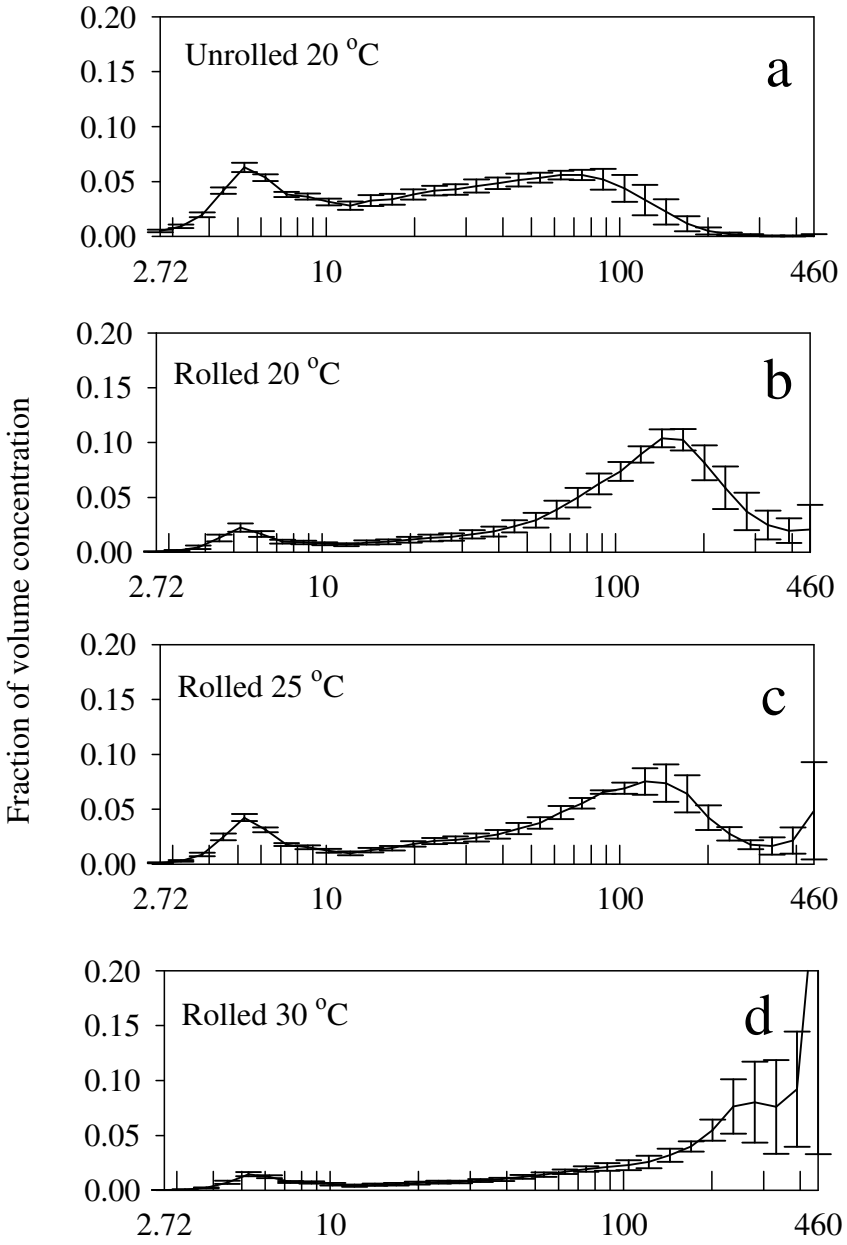

Fig. 17. Particle size distributions (PSD) of four independent *S. costatum* cultures incubated at different temperatures. PSDs normalized to total volume concentration represented by curves drawn through mean values ± SD (n = 400). (a) and (b) were incubated at 20°C. (c) incubated at 25°C (d) incubated at 30°C. Figure b, c, and d were gently rolled inside dark bottles during incubation to enhance particle collision.

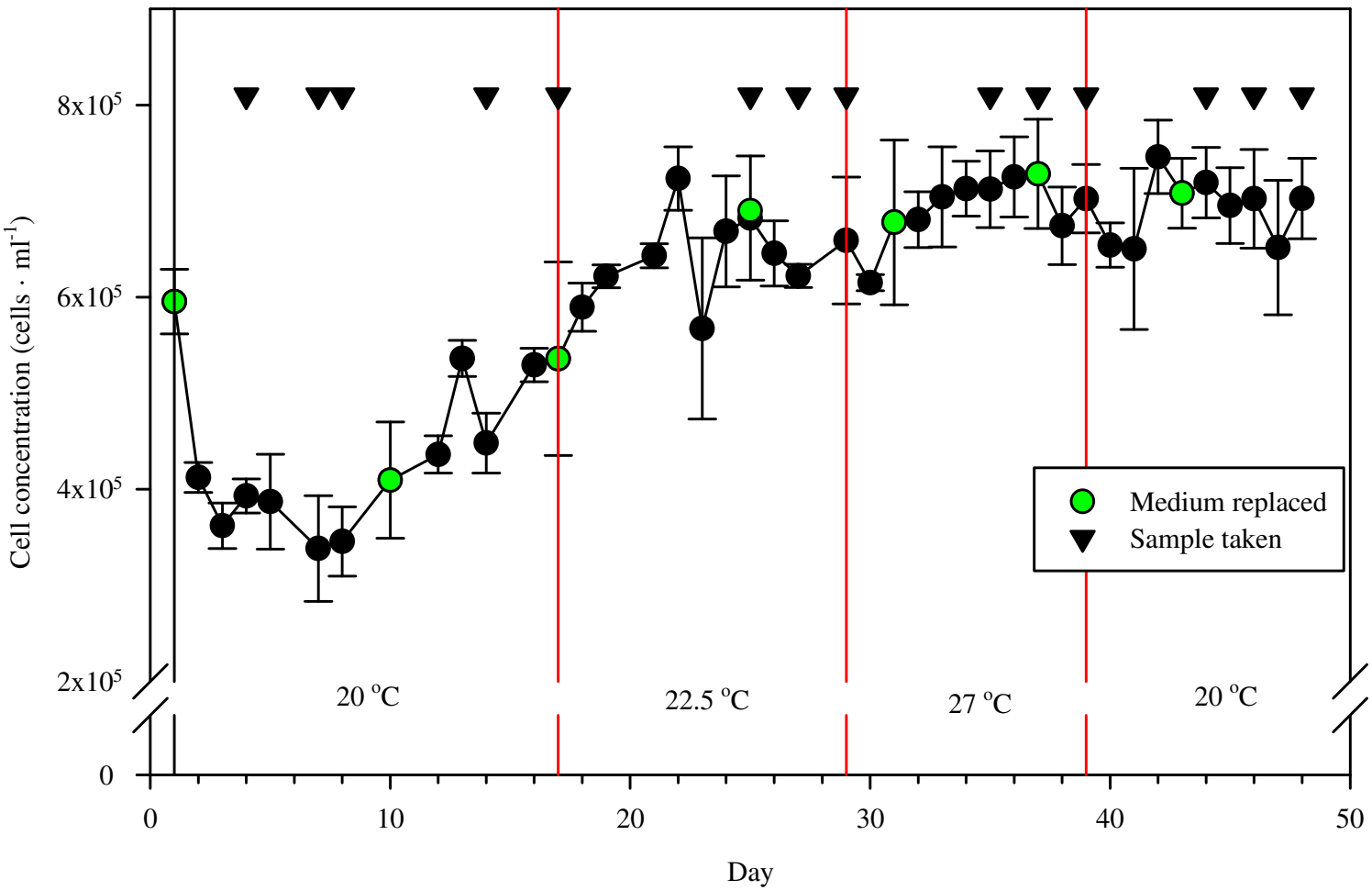

Fig. 18. Chemostat timeline showing cell concentration (mean ± SD) from day 1 to day 48. Black vertical reference line indicates when the dilution was started. Red reference lines demarcate temperature change regions. Black triangles indicate a day when full sample from the four chemostat cultures for cell counts, chlorophyll *a*, total carbohydrates, LISST PSD and prokaryote counts. Green circles indicate when the medium carboy was replaced with new medium.

Table 4. Chemostat Pearson Product Moment correlation coefficients. Bolded values represent statistically significant correlations $p < 0.05$ ($n = 4$).

	Measured temp	Cell counts	Prokaryote count	Prokaryote/cell	Total Carbs	Carb/cell	Chl	Chl/cell	APS area	APS area per cell	# of APS particles	LISST volume
Culture #	-0.00215	-0.152	-0.0869	-0.0316	0.0101	0.0479	0.00412	0.0299	0.00895	-0.0365	-0.0374	-0.319
Day	-0.318	**0.253**	0.306	-0.421	-0.152	-0.331	-0.0438	-0.21	-0.266	-0.3	-0.0925	-0.284
Measured temp	--	0.135	0.0558	-0.0842	**0.878**	**0.817**	**0.672**	**0.603**	**-0.523**	**-0.488**	-0.72	0.0332
Cell counts	--	--	0.725	-0.144	0.163	-0.203	0.203	-0.239	**-0.339**	**-0.444**	**-0.244**	-0.18
Prokaryote count	--	--	--	0.497	0.219	-0.0387	0.16	-0.309	-0.533	-0.568	-0.165	-0.632
Prokaryote/cell	--	--	--	--	0.0453	0.144	-0.184	-0.114	-0.176	-0.171	0.0849	**-0.424**
Total Carbs	--	--	--	--	--	0.931	0.539	0.464	-0.489	-0.461	-0.647	-0.138
Carb/cell	--	--	--	--	--	--	**0.457**	**0.541**	**-0.353**	**-0.294**	**-0.535**	-0.0901
Chl	--	--	--	--	--	--	--	**0.901**	**-0.612**	-0.589	**-0.693**	-0.0438
Chl/cell	--	--	--	--	--	--	--	--	**-0.465**	**-0.392**	**-0.579**	0.0404
APS area	--	--	--	--	--	--	--	--	--	**0.99**	**0.796**	0.429
APS area per cell	--	--	--	--	--	--	--	--	--	--	**0.761**	**0.47**
# of APS particles	--	--	--	--	--	--	--	--	--	--	--	**0.136**

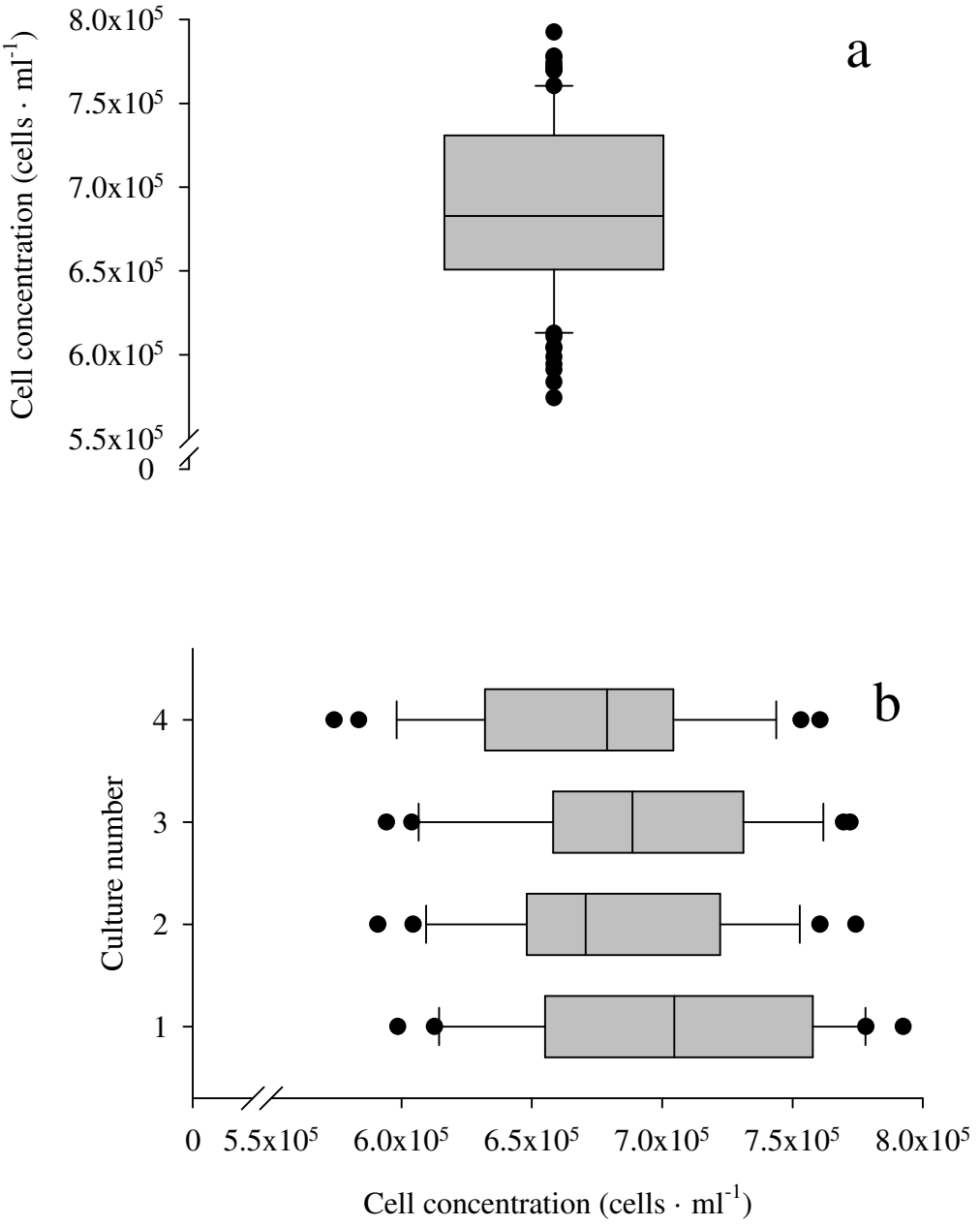

Fig. 19. Box plots showing average cell concentration and cell concentration per culture. (a) Box plot shows concentration values from all culture during steady state (Day 25-48). (b) Cell concentrations from each culture flask during steady state (Day 25-48). Left boxes and right boxes are separated by median value line and represent 25th and 75th percentile, respectively. Whiskers represent the 99th percentile. Black points are outliers.

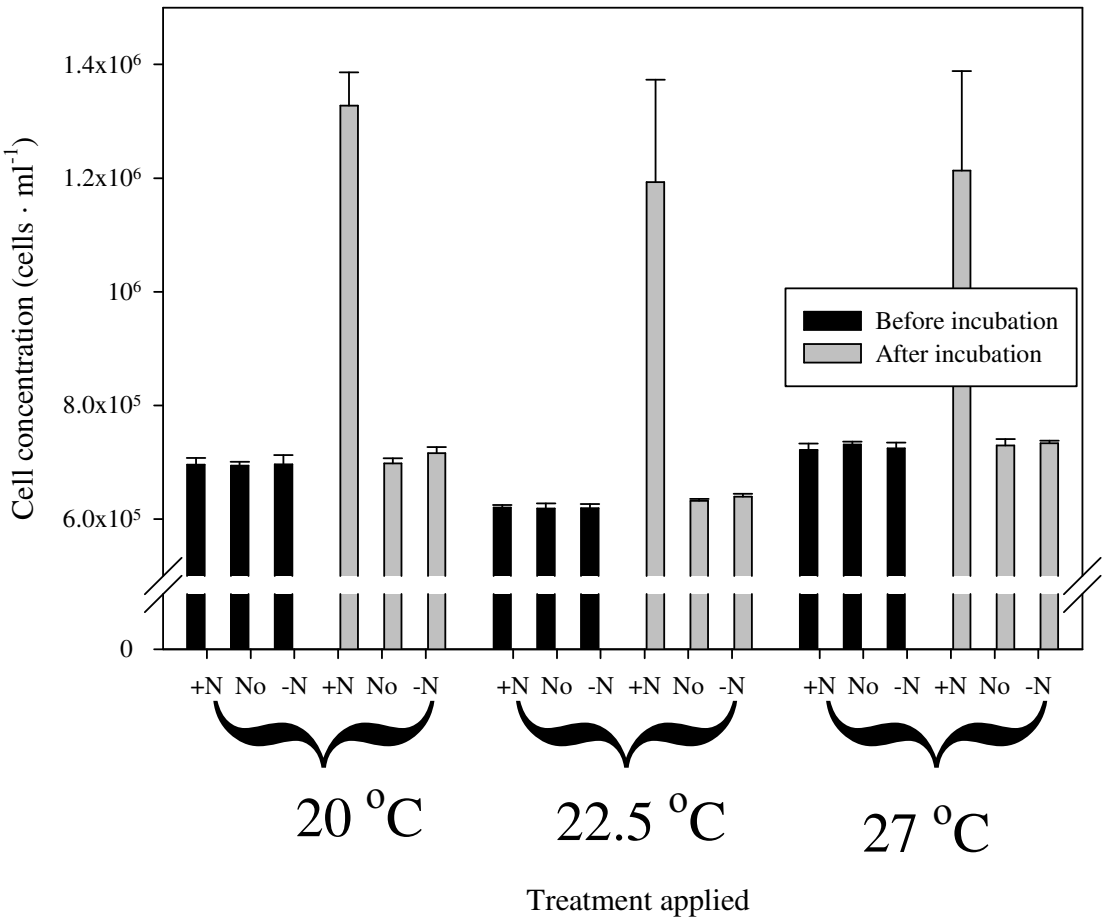

Fig. 20. Bioassay cell concentrations from each temperature verifying nitrogen limitation. Cell concentrations are reported as the mean ± SD across all cultures (n = 4). Bioassays were treated with nitrogen (+N), no nutrients (No), and all nutrients except nitrogen (-N).

Evidence that cultures were nitrogen-limited is shown in Fig. 20 where 40 ml replicate culture vials were treated with no addition of nutrients, addition of final concentration 100 µM $NaNO_3$, or addition of all nutrients according to final concentrations in Table 2 without addition of $NaNO_3$. After a 48 h incubation at 24h light, the 20, 22.5 and 27°C cultures that were treated with the addition of nitrogen showed two-fold increases in cell concentrations, greatly surpassing the pre-incubation average cell concentrations.

Total carbohydrate and chlorophyll *a* values with time are shown in Fig. 21a and Fig. 22a. While chlorophyll *a* remains relatively constant at 22.5°C and during second 20°C temperature period, both chlorophyll and carbohydrates increased during the 27°C period. Total carbohydrate concentrations, however, differentiate themselves from the trend exhibited by chlorophyll, maintaining higher mean values at 22.5 than at 20°C. According to Table 4, both total carbohydrates and chlorophyll correlate significantly ($p<0.05$) with temperature.

When staining acid polysaccharides (APS) with alcian blue, the expectation was to observe transparent exopolymer particles (TEP), which would either be independent of the cells or contain cells embedded within them. What was actually evident on the stained filters were a small number of APS particles, with most of the alcian blue staining appearing as a coating on the surface of the cells (Fig. 23) indicating that acid polysaccharides coated the cell surfaces. *C. muelleri* cells can be noted to be stuck together in a web-like, blue matrix. Under brightfield microscopy at 100x magnification, it is often difficult to directly observe the spines of *C. muelleri* but after

staining, both the main body of the cell and its spines were easily visible, indicating that the spines were covered in a layer of APS. While it is unknown as to whether the cells were stuck together as a result of cell surface stickiness or simply became stuck together during filtering, Figure Fig. 23a shows the simplest form of this structure, one cell attached to the next by the sticky coating that allowed the spines to be stained and visible as blue. These APS matrices vary in size, shape and intensity of staining throughout the length of the experiment with temperature changes. Figure Fig. 23b from a chemostat vessel at 27°C highlights both the matrix-like nature of *C. muelleri*, the intensely dark staining of the cells themselves, but also the tiny, stained particles present throughout the matrix.

When images were analyzed for APS particles using ImageJ software analysis from the National Institute of Health, hundreds of thousands of particles resulted, varying in size from 0.412 μm^2 all the way to 10's of thousands of square micrometers. Particles sized at 0.412 μm^2, or the area of a single pixel, accounted for over 25% of total particle number and total particle area. It was decided that single pixel particles at 100x magnification could not be discerned from background noise and were, therefore, excluded from the data analysis.

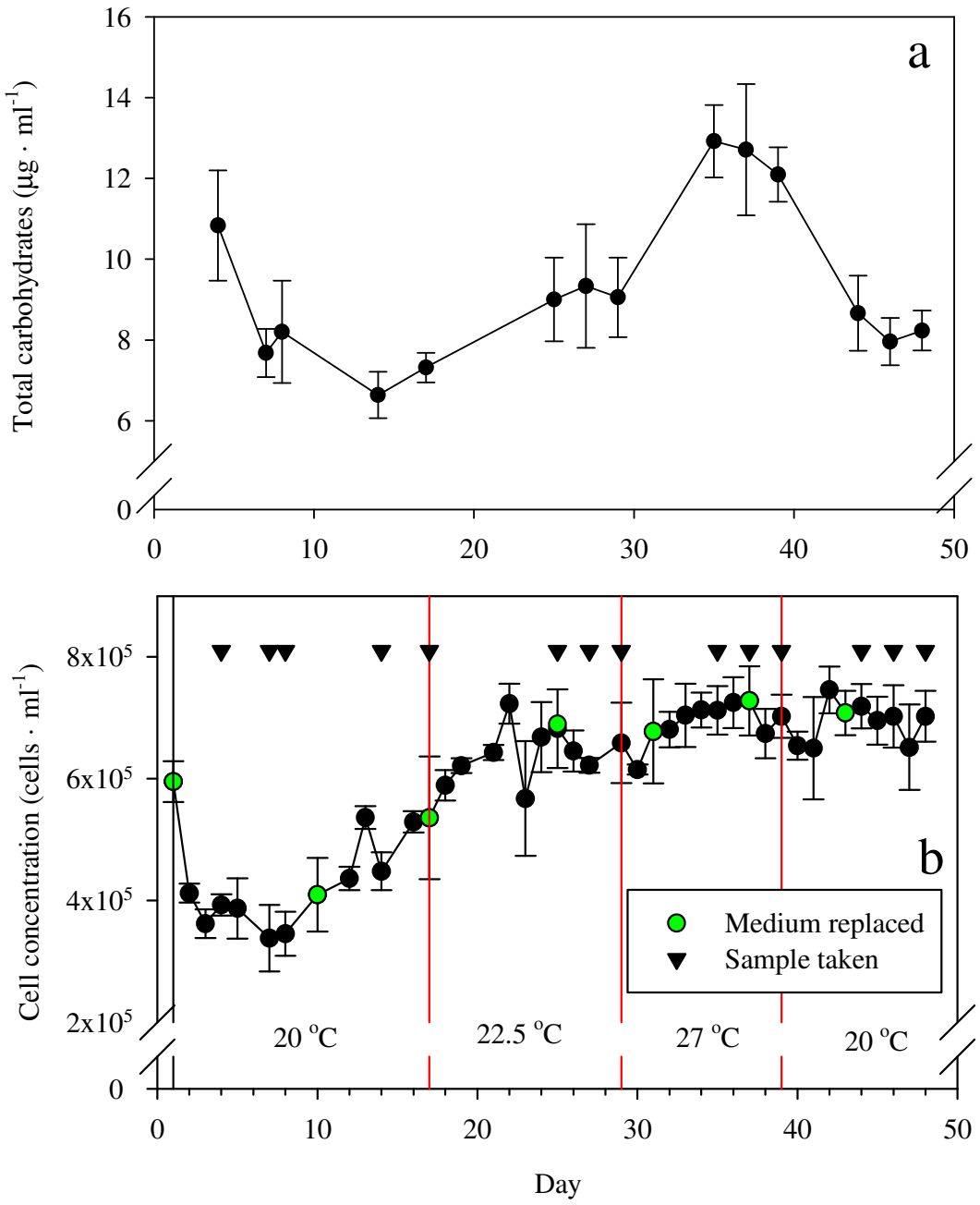

Fig. 21. Total carbohydrate concentrations in chemostat. (a) Total carbohydrate values (mean ± SD; n = 4) with time (b) Chemostat timeline showing cell concentration (mean ± SD) from day 1 to day 48. Black vertical reference line indicates when the dilution was started. Red reference lines demarcate temperature change regions. Black triangles indicate a day when full sample from the four chemostat cultures for cell counts, chlorophyll *a*, total carbohydrates, LISST PSD and prokaryote counts. Green circles indicate when the medium carboy was replaced with new medium.

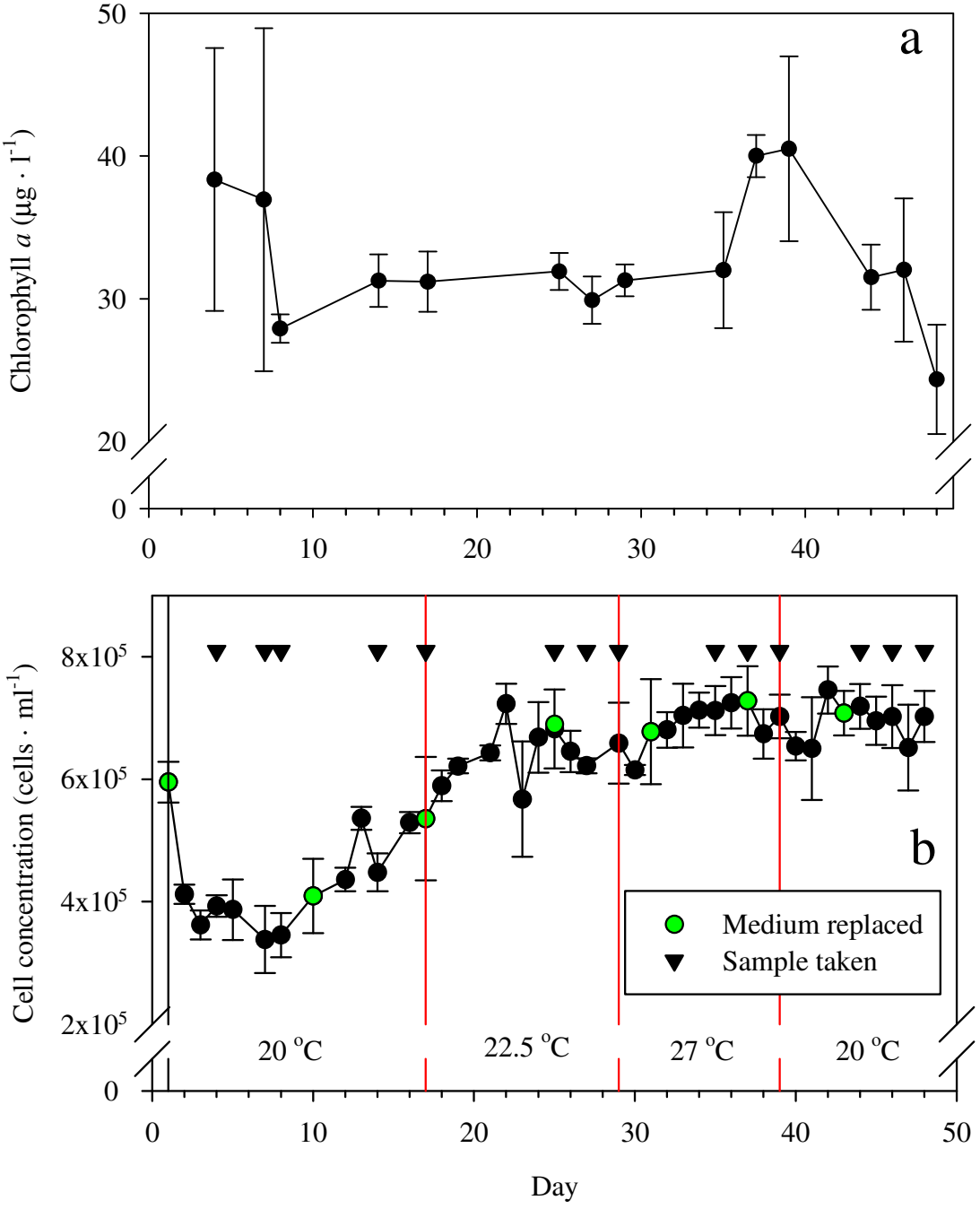

Fig. 22. Chlorophyll *a* concentrations in chemostat. (a) Chlorophyll *a* concentrations (mean ± SD; n = 4) with time (b) Chemostat timeline showing cell concentration (mean ± SD) from day 1 to day 48. Black vertical reference line indicates when the dilution was started. Red reference lines demarcate temperature change regions. Black triangles indicate a day when full sample from the four chemostat cultures for cell counts, chlorophyll *a*, total carbohydrates, LISST PSD and prokaryote counts. Green circles indicate when the medium carboy was replaced with new medium.

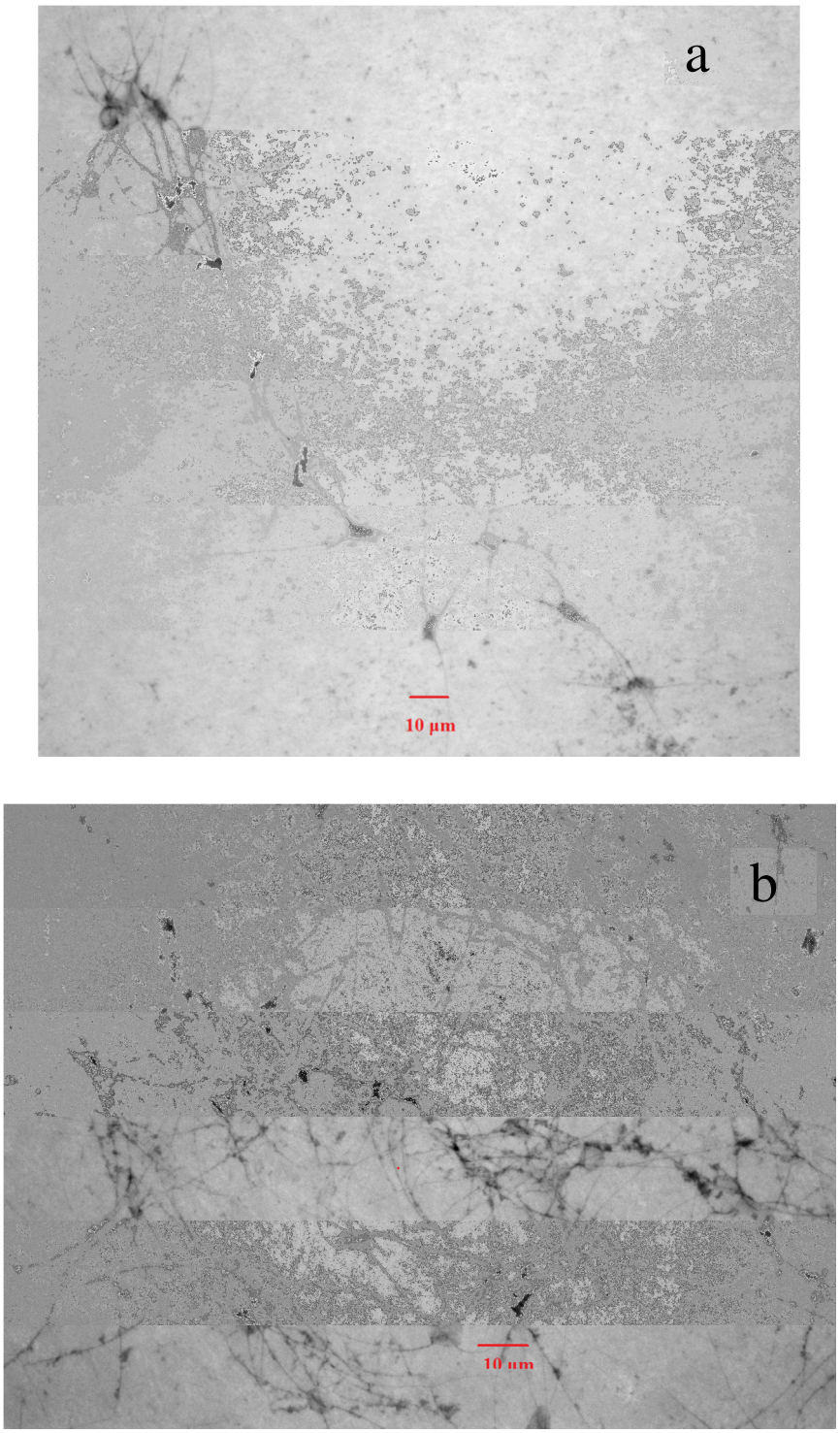

Fig. 23. Alcian blue-stained *C. muelleri* cells at 400x magnification at 27°C (a) Demonstrates the simplicity of how each diatom will stick to one another (b) Dense, darkly-stained cell matrix. Note presence of small stained particles caught within the sticky matrix only resolved at 400x magnification.

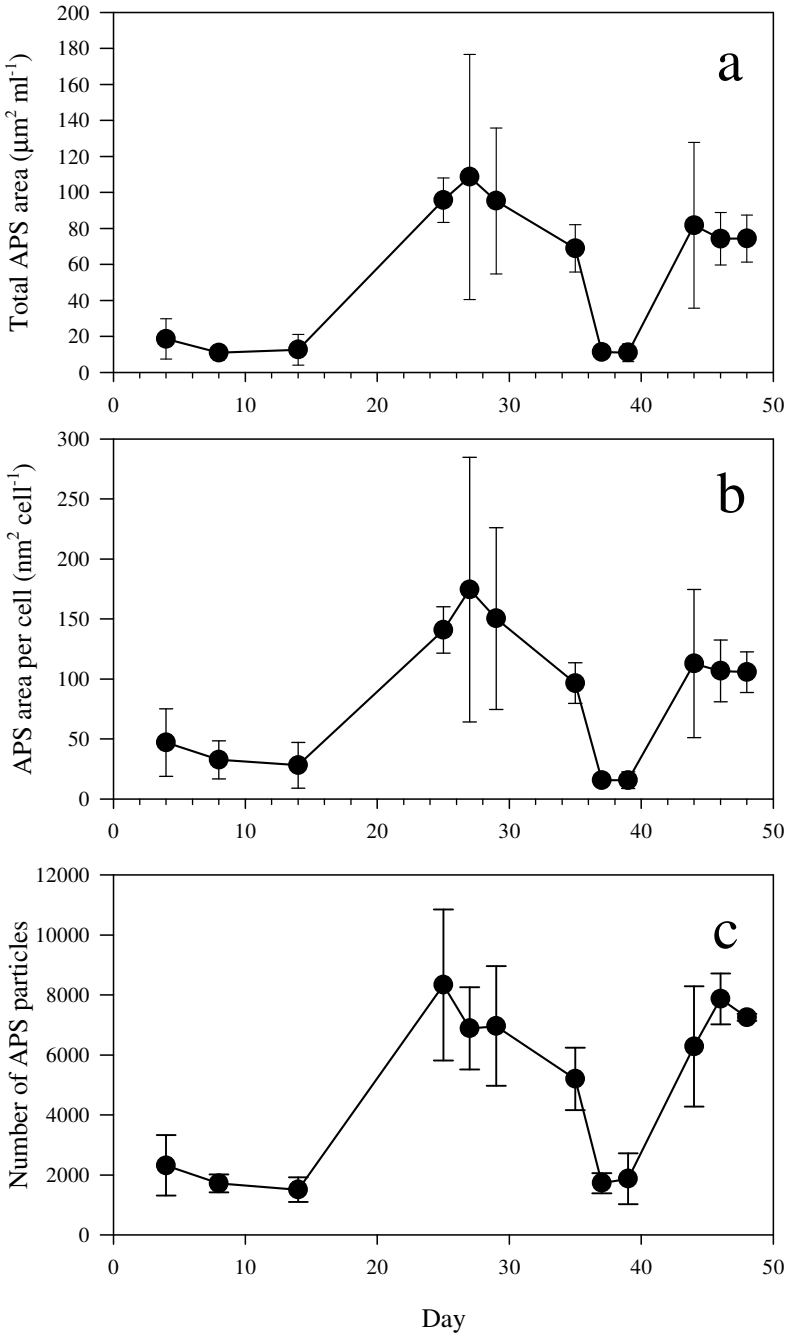

Fig. 24. APS concentrations over time in chemostat. Data points are mean ± SD; n=4 (a) Total APS area (b) APS area as a function of cell concentration (c) Number of APS particles.

Fig. 24 depicts the same trend through each temperature change. During the first 20°C period, APS was very low throughout but as biomass increased toward steady state past day 17, APS in all three figures increased proportionally. APS remained steady for the sampling period at 22.5°C but as temperature changed to 27°C at day 29, APS decreased in all three categories remaining low in value until temperature was lowered to 20°C and APS appears to steady until the end of the experiment. Interestingly, APS area and number of APS particles behaved differently when temperature was lowered to 20°C with total APS area lowering to values below what was achieved at 22.5°C, while number of APS particles rose back to comparable values achieved at 22.5°C. Indeed, APS values in terms of total area or total area per cell were significantly correlated with measured temperature $r = -0.720$, $p = 1 \times 10^{-6}$, $n = 35$ and values $r = -0.727$, $p = 7 \times 10^{-6}$, $n = 35$, respectively, number of APS particles was not significantly correlated $r = 0.0332$, $p = 0.850$, $n = 35$. Carbohydrate and APS also exhibit an interesting relationship. According to Fig. 29, APS per cell both decreases and becomes less variable as a function of increasing carbohydrate per cell. LISST PSDs throughout each temperature period, normalized to total volume detected during each temperature period, were compared to the second 20°C period (day 39-48) when cultures were considered to be in steady state. Fig. 25a, Fig. 25b, and Fig. 25c illustrate the baseline set during that 20°C period and then the net mean changes in volume concentration when temperatures change to 22.5 and 27°C, respectively.

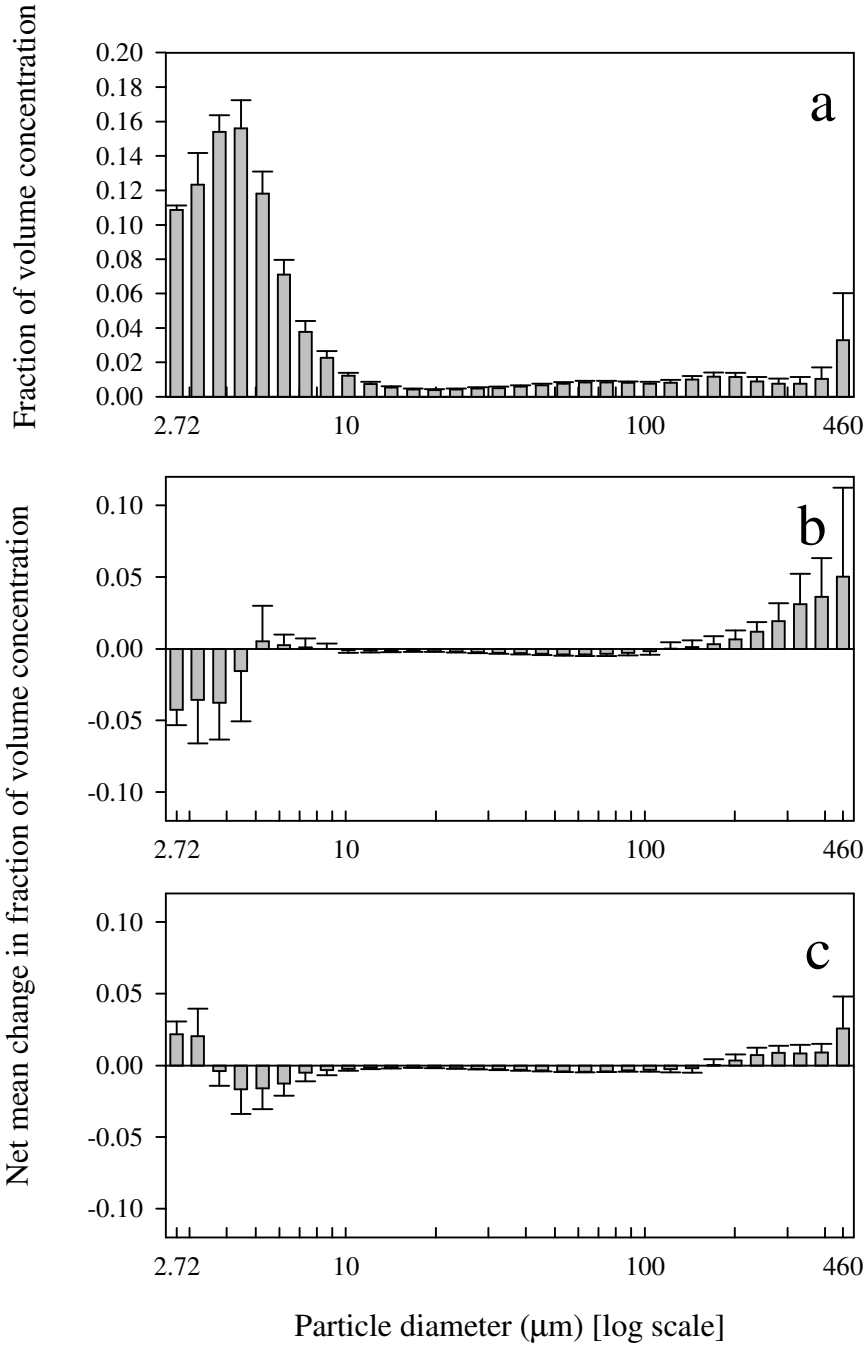

Fig. 25. Net changes in LISST volume with temperature. Bars represent mean SD (n = 12) (a) 20°C baseline (n = 400) (b) 22.5°C net mean change in volume concentration from 20°C (n = 4) (c) 27°C net mean change in volume concentration from 20°C (n =4).

In Fig. 13a, as with the *C. muelleri* LISST measurements featured in Figure Fig. 13a, a wide peak centered around 4 µm includes both the major and minor axis of a single *C. muelleri* cell. Fig. 25b at 22.5°C shows a net change in both the large and small size bin ranges with a decrease in the central peak height by approximately 4% and an increase in the large size bin range from 100 µm to 460 µm of nearly 5%. Figure Fig. 25c from 27°C depicts a similar trend with decrease in the central peak and an increase in the large size bins. However, both the 2.72 and 3.20 µm size bins show a net increase in volume concentration of 2%.

Prokaryote cell concentration is shown in Fig. 26. Prokaryote counts were taken during each sampling day but only the median day during temperature periods were counted. Bars in Fig. 26 show the mean concentration + SD (n = 4). While measures were taken to eliminate prokaryote from the chemostat cultures, concentration remained fairly constant throughout and did not correlate with either diatom concentration or temperature. This shows that chemostat cultures did not remain prokaryote free as intended. Despite the concentration of prokaryotes not correlating significantly with temperature, prokaryotes have the potential not only to use or remineralize nutrients intended for the diatom cultures but to affect the level of total carbohydrates detected.

Integrated LISST volume concentration (Fig. 27) appeared to follow a similar trend as with chlorophyll, carbohydrates, and APS, but range of concentrations seen during the period from day 17 to day 27 making resolving overall trends difficult. Throughout the experiment, the silicone nutrient lines leading to each culture vessel were found to gather and bind precipitate from the medium. To prevent the precipitate

from fouling the culture vessels, the lines were cleaned and autoclaved every six days or each occasion the main medium carboy was replaced. Precipitate was observed to break from the lines and enter vessels on day 17, but was also observed leaving through the waste lines. While no precipitate was visible inside the culture vessels from day 17 to day 27, Fig. 28 shows integrated LISST volume for each culture vessel, highlighting the large deviation of culture 1 from the trend and volume concentration values exhibited by culture 2, 3, and 4. Precipitate within all the culture flasks likely influenced the LISST volume concentrations if only in the largest size bins. Despite the deviation of culture 1 seen in Fig. 28, the upward trend in total volume can still be seen at 27°C as it comes back down to lower levels at 20°C and integrated LISST volume was found to significantly correlate with temperature change ($r = -0.448$, $p = 3 \times 10^{-3}$, $n = 4$), though possibly as a direct result of culture vessel 1's deviation (Table 4).

When plotting the measured temperature within each culture vessel against total carbohydrate per cell (Fig. 29) a positive, linear trend results when temperature increases, total carbohydrate within the vessel increases. When including data only within steady state (Day 25-48), the differences in the median carbohydrate per cell values among each temperature are highly significant $p < 0.001$ (Kruskal-Wallis one-way ANOVA on ranks). However, the relationship between carbohydrate per cell at 27°C and 20 or 22.5°C is significant $p < 0.05$ (Tukey Test), while the carbohydrate values for 22.5°C are not significant when compared to 20°C $p > 0.05$ (Tukey Test).

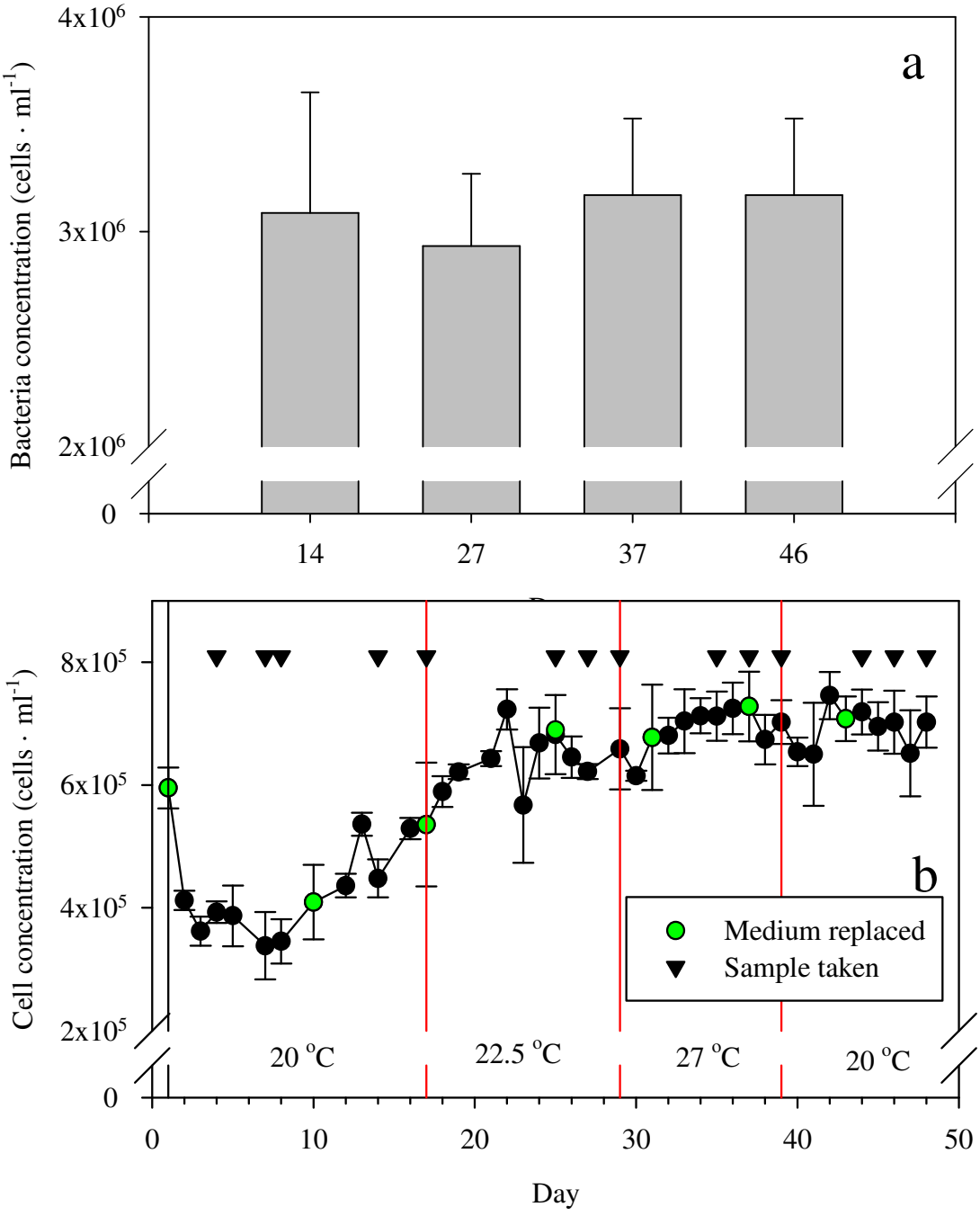

Fig. 26. Prokaryote cell concentrations in the chemostats. (a) Prokaryote concentrations (mean + SD) (n = 4) with time (b) Chemostat timeline showing cell concentration (mean ± SD) from day 1 to day 48. Black vertical reference line indicates when the dilution was started. Red reference lines demarcate temperature change regions. Black triangles indicate a day when full sample from the four chemostat cultures for cell counts, chlorophyll *a*, total carbohydrates, LISST PSD and prokaryote counts. Green circles indicate when the medium carboy was replaced with new medium.

Overall trends with temperature were investigated through the construction of a dendrogram using classification analysis in Fig. 30. Cultures vessels, paired with temperature, were analyzed using values for diatom cell concentration, chlorophyll per cell, carbohydrate per cell, APS area per cell, and prokaryote cell concentration acquired during days 14, 27, 37, and 46. The horizontal distance between branching points represent how similar paired cultures are to one another. By far, the largest visible distance in relationship is between all four cultures at 27°C and cultures at every other temperature. Because the 27°C cultures all branched at such a small distance, this implies that the similarity between each individual culture was much greater at this temperature than any other. Cultures at 20°C all share the same distance in relationship as well, cultures 3 and 4 at 22.5°C branch off to share the same relatedness to 20°C. However, cultures 1 and 2 at 22.5°C share the same distance in relationship to cultures 1 to 4 at 20°C and 3 to 4 at 22.5°C. This indicates that while there was a large difference between all cultures at 27°C when compared to 20°C, in terms of LISST volume, chlorophyll *a* per cell, carbohydrate per cell, APS per cell, cell concentration and prokaryote concentration, there was no difference between cultures at 22.5°C and 20°C.

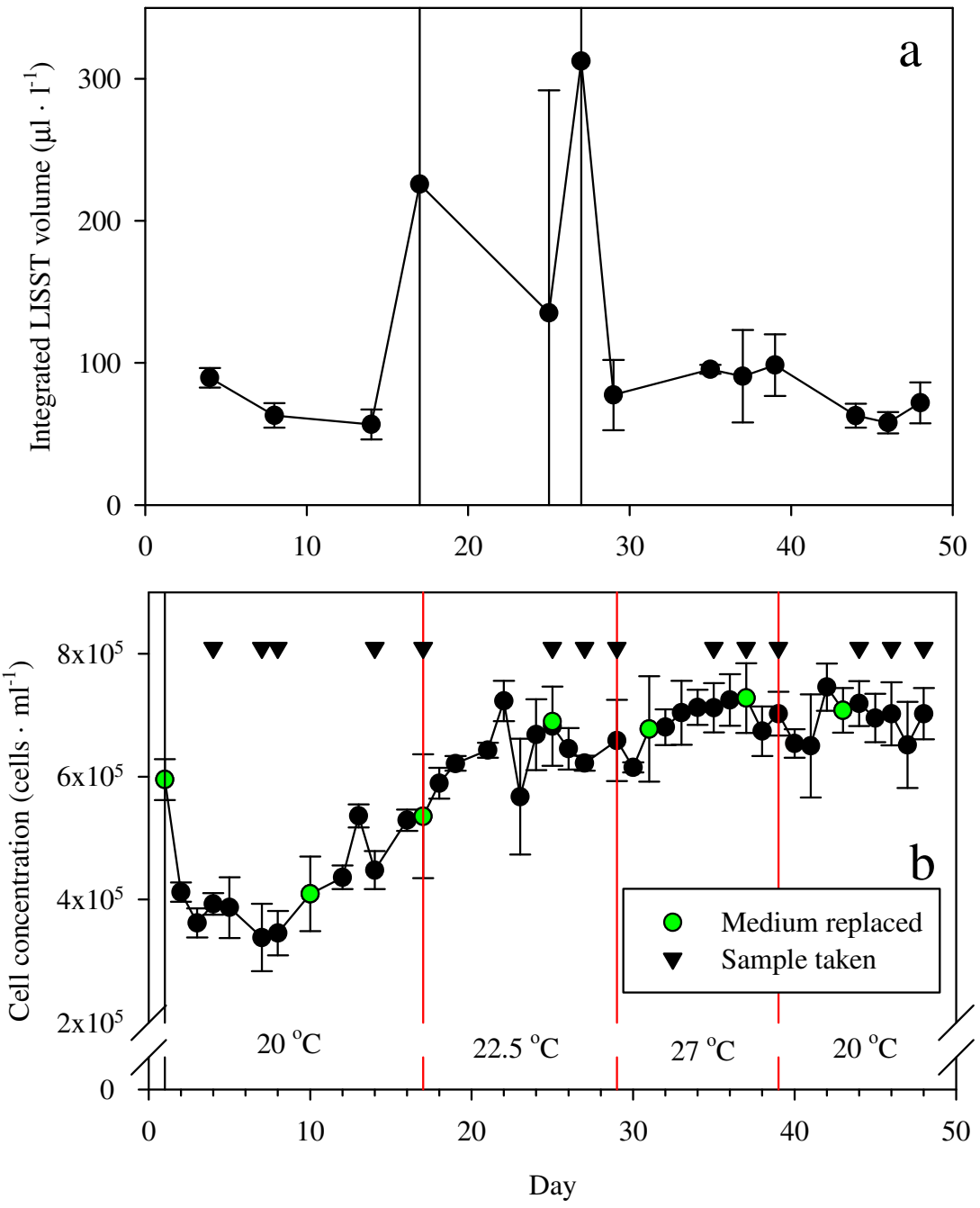

Fig. 27. Integrated LISST volume in chemostat. (a) Integrated LISST volume pooled from four independent cultures with time (mean ± SD; n = 400) (b) Chemostat timeline showing cell concentration (mean ± SD) from day 1 to day 48. Black vertical reference line indicates when the dilution was started. Red reference lines demarcate temperature change regions. Black triangles indicate a day when full sample from the four chemostat cultures for cell counts, chlorophyll *a*, total carbohydrates, LISST PSD and prokaryote counts. Green circles indicate when the medium carboy was replaced with new medium.

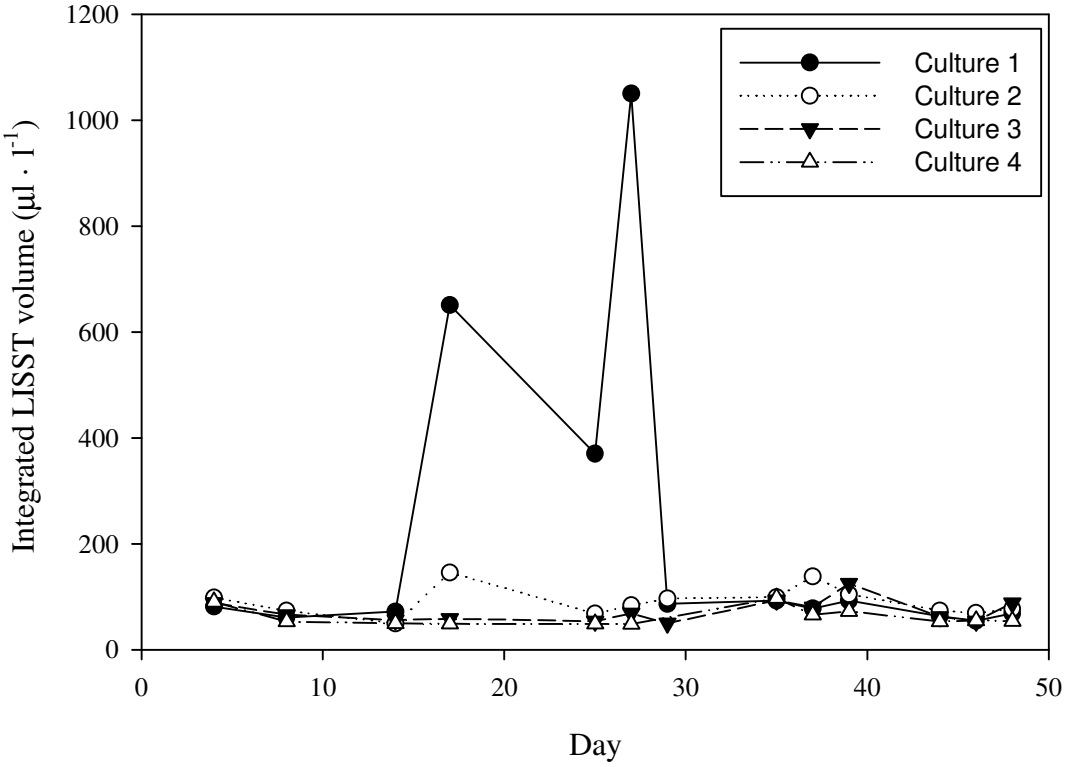

Fig. 28. Integrated LISST volume per culture in chemostat. Each line represents an individual culture's integrated LISST volume (n = 100) with time.

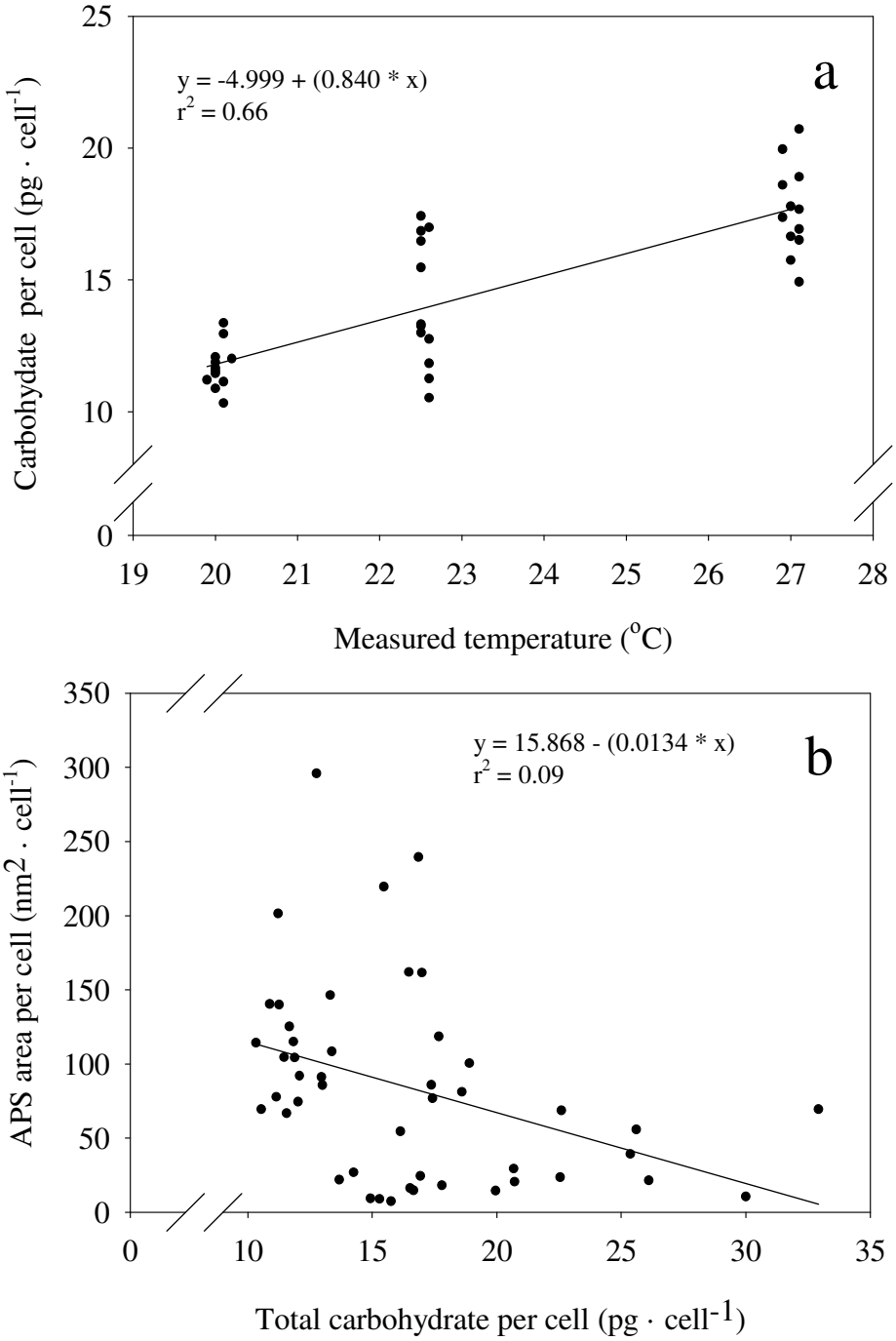

Fig. 29. Relationships between carbohydrates and APS. (a) Relationship between measured temperature during steady state (Day 25-48) and carbohydrate per cell ($r^2 = 0.66$) (b) Relationship between APS area per cell and total carbohydrate per cell ($r^2 = .09$)

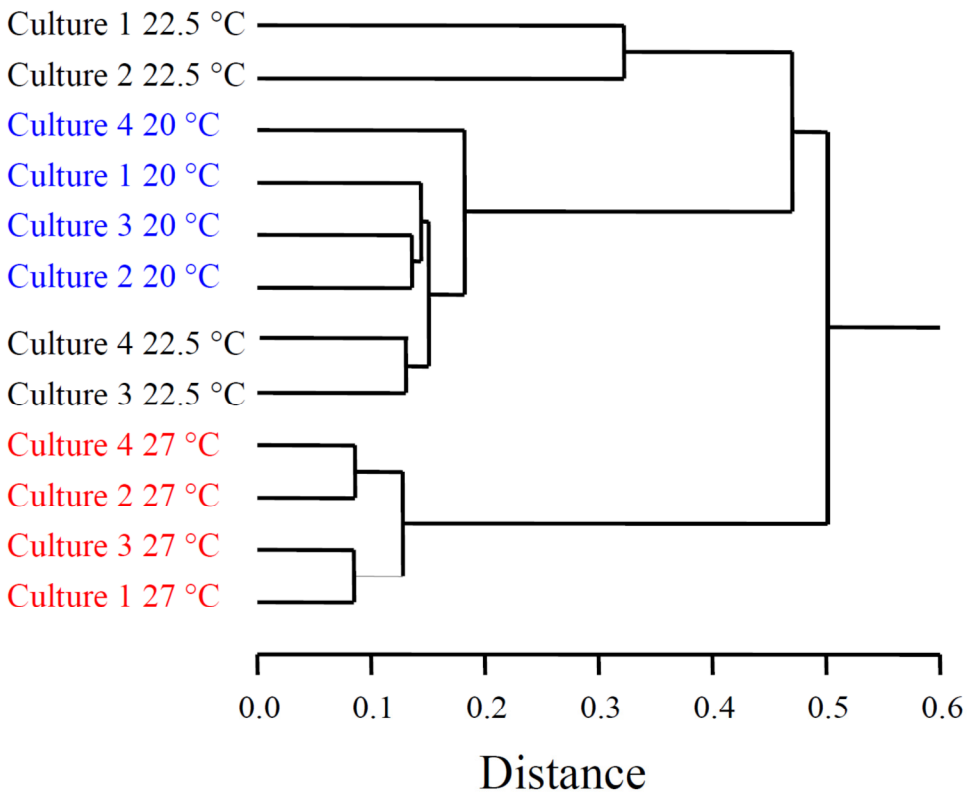

Fig. 30. Classification analysis of chemostat data. Data was only taken from days 14, 27, 37, and 46 when prokaryote counts were taken. This dendrogram shows the relationship of each culture and a paired temperature to each other using data from prokaryote counts, cell counts, carbohydrate per cell, chlorophyll per cell, APS area per cell, and LISST total volume concentration. The x-axis represents distance in terms of similarity: the shorter the distance for a branching point, the more similar the branches are to each other.

4. DISCUSSION AND CONCLUSIONS

4.1 The LISST as a tool to identify diatoms and their aggregates

The microsphere experiment was used to determine how the LISST size and quantify a simple and precise object, the sphere. Each of the 6, 25, and 90 µm microsphere particle size distributions featured single, narrow peaks occupying several size bins. However, the polystyrene microspheres (Duke Scientific, Inc. Palo-Alto, CA) are NIST-traceable and had very tightly constrained diameters and suspension concentrations. Therefore, particles will occupy several size bins not because of inherent variation in microsphere diameter but because the mathematical models used by the LISST limit the resolution of particle size class detection, allowing leakage of particle volume to adjacent size bins (Agrawal and Pottsmith 2000). When a 25 µm spherical particle was detected, it was categorized to belong within a range of bins, with median diameters of 23.4 and 27.6 µm. Particles slightly smaller and slightly larger than precisely 25 µm were assigned to size bins adjacent to 23.4 and 27.6, still comprising a single peak. The 6 and 90 µm microspheres being closer to the median of a single size bin had the majority of particle volumes assigned to a single size bin, but still sharing total volume concentration between adjacent size bins. Moreover, in the case of the 25 µm microspheres, LISST total volume concentration was shown to have a significant, linear relationship with actual bead concentration. The LISST cannot detect the exact diameter of a spherical particle but instead categorizes it to belong to a range of diameters, where the median of each of the 32 ranges between 2.5 and 500 µm is 1.18

times the previous range, along a logarithmic scale. Despite what appeared to be imprecise volume measurement and size ranking by the LISST, dilutions produced both precise and accurate measurement of a microsphere suspension that agrees with previous testing (Agrawal and Pottsmith 2000; Gartner 2001). While the LISST 100X is not greatly affected by a particles' refractive index (Agrawal and Pottsmith 2000), previous testing using the LISST has only been briefly conducted on diatoms, purple sulfur bacteria, and dinoflagellates (Serra et al. 2001; Karp-Boss et al. 2007; Angles et al. 2008; Rienecker et al. 2008). While Serra et al. (2001), Karp-Boss et al. (2007), Angles et al. (2008), and Rienecker et al. (2008) all had success detecting these organisms, I was unsure how a diatom's varied relative dimensions and aspect ratios would be represented in a particle size distribution. Each diatom species was grown and sampled during periods where a culture may be assumed to exhibit differences in cell size, culture density or other unknown factors: growth, lag, and stationary phases. Because a visual inspection of culture flasks was used to determine when each phase began, the start exponential growth phase of each diatom was overestimated, causing them to be sampled after the phase had begun. As biomass was different for each culture and across species, it became important to correct for differences in volume concentrations so not only different species be compared to one another but also single species could be compared to themselves over time. By normalizing the volume of each size bin to the total volume of all size bins, this made comparison in peak heights and peak distributions amongst the particle size distributions (PSD) possible, highlighting how a species' dimensions may change or illustrate how a relative volume in each bin may be

allocated differently. While each diatom's PSD had tightly constrained standard deviations across the 900 measurements averaged to produce them (Fig. 13 and Fig. 14), only those diatoms with large aspect ratios generated multi-peak PSDs. *Coscinodiscus wailesii*, *Chaetoceros muelleri* and *Thalassiosira weissflogii* have different major and minor axes but only produce single peaks. The *Skeletonema costatum* and *Skeletonema marinoi* PSDs had peaks corresponding to both single-cell and multi-cell major and minor axes but were indistinguishable from one another. *Phaeodactylum tricornutum*, a pennate diatom, produced a distinct PSD based on its major and minor axes. Therefore, PSDs generated from a diatom would be unreliable to identify diatom species from one another but can easily identify between centric, pennate, chain-forming diatoms. Moreover, the LISST only records volume concentrations for each size bin range, so this data was manipulated to calculate the number of particles and surface area of particles within each size bin range (Fig. 13). The combination of these three distributions could serve as further identifying features: Fig. 13a, Fig. 13b, and Fig. 13c for *Chaetoceros muelleri* vary greatly from Fig. 13d, Fig. 13e, and Fig. 13f from *Coscinodiscus wailesii*.

To demonstrate the LISST's ability to detect changes in a particle size distribution (PSD), two factors were introduced to induce aggregation in *Skeletonema costatum* cultures: rolling of culture bottles and temperature change. Aggregation of the cultures would be evident when the proportion of small particles would decrease and the proportion of large particles would increase. In Fig. 17, simply through rolling the cultures, clear differences appeared in how volume concentration was allocated in size bins. *S. costatum* is a chain-forming diatom, its PSD reflects peaks for not only single

cell dimensions but also peaks corresponding to the dimensions of multi-cell chains. It is likely that through the action of rolling, single cells, as well as cell chains, had increased collision rates, becoming tangled as a result. This would explain the increase in volume concentration around the 100 μm size bins and decrease in volume at the lower size bins for 20°C (rolled). At 25°C, again, particle volume around the 100 μm size bin remains high in relative concentration, but drawing distinction between the PSD at 20°C (rolled) and 25°C (rolled) is difficult. The temperature increase to 30°C, however, accentuates the increase in particle diameters and volume concentrations in the large particle size bins even further. Fig. 17d at 30°C shows the largest decrease in the peak centered around 4 μm and a shift in volume from near the 100 μm size bin to 300-500 μm. We had hypothesized that the LISST could be used to investigate the formation of aggregates. Although the trend at 30°C deviates from the PSD displayed at the cooler temperatures, these results mirror what Thornton and Thake (1998) have shown before: incubating *S. costatum* at increased temperatures results in increased aggregate concentration. Our results deviate from those of Thornton and Thake (1998), however, in that the LISST PSD at 30°C does not indicate a higher concentration of aggregates but rather the formation of larger aggregates. 30°C is a very warm temperature to incubate a diatom when the diatoms had previously been acclimated to 20°C for many generations. If the cultures incubated at high temperature lysed, the leaking cell contents may have enhanced the stickiness of the particles, allowing the aggregates to grow greater in size. While the reasons are unclear as to why aggregates formed, this example demonstrates

the LISST can effectively detect subtle changes in volume concentrations, verifying its usefulness in aggregation formation studies.

4.2 Chemostat cultures

Being the first study to investigate aggregation in marine diatoms using the LISST, this experiment is also the first to look at the effects of temperature on transparent exopolymer particles (TEP) production using a nitrogen-limited continuous culture system. The success of this continuous culture experiment was dependent upon our ability to keep it nitrogen-limited and keep diatom biomass in steady state.

Nitrogen limitation was maintained successfully and shown in the bioassay cell concentrations in Fig. 20. Treatments that were incubated with the addition of nitrogen (+N) showed two-fold increases in cell concentration at three temperatures versus those where no nutrients (No) or all nutrients without nitrogen (-N) where no significant increase in biomass was observed.

Historically, continuous culture steady state has been defined as when specific growth rate (μ) is equal to total loss rate of phytoplankton through dilution rate (D) (Monod 1950; Andersen 2005). Steady state of the chemostat culture for this experiment was defined as when cell concentrations day-to-day did not vary by more than 10%. As the cultures adjusted to the growth at the start of medium dilution, it was assumed that the system was in steady state on day 3. However, cell concentrations continued to increase and only after day 25 were the cultures deemed to be in steady state with average cell concentration variation between vessels being 6%.

4.3 Prokaryote contamination in chemostat

As shown in Fig. 26, prokaryote counts during just four days of the chemostat reflect the large presence (> 10^6 cells · ml^{-1}) of prokaryotes in all four culture vessels. Samples for prokaryotes were not taken during at the start of dilution so it is unknown if the cultures were contaminated at the experiment's start or if prokaryotes were introduced over time. Prokaryote concentrations did not vary significantly with diatom cell concentration and did not vary significantly with temperature. There are three main possibilities for the introduction of prokaryotes into the system: air contamination, nutrient medium contamination, or contamination during sampling. While strict sterile technique, underneath a positive flow hood, was used to sample from the culture vessels, only filtration was used to sterilize both the air and nutrient medium. Air was filtered through triply-redundant sterile 0.2 µm filters but filters were not changed or re-sterilized during the experiment. Nutrient medium was changed frequently but only filtered through sterile 0.2 µm filters and not autoclaved. Autoclaving the artificial seawater prior to nutrient addition was not possible due to space requirements needed to autoclave 20 L of medium. Despite the space requirements, autoclaving would likely have not been used as artificial seawater salt had been observed to precipitate after autoclaving. Therefore, while it may have been possible that prokaryotes survived the antibiotic treatments of each culture vessel, it is more likely that prokaryotes were introduced as a result of passing through sterile filters. Prokaryotes abundance, while not significantly correlating with APS or carbohydrates in this experiment, could have large implications with either production of APS or the use of APS as a substrate. It has

been shown that while TEP did not appear as a carbon substrate being used by bacteria, TEP might have a weak, inverse correlation with total bacterial abundance (Bhaskar and Bhosle 2006). Additionally, prokaryotes could also affect total carbohydrate concentrations not just because they may use carbohydrate as substrate but because prokaryote cell biomass itself would be included in total carbohydrate measurements. Prokaryotes may also have competed with diatoms for essential nutrients such nitrogen or phosphorous and prokaryote growth may have released metabolic toxins prohibitive to diatom growth.

4.4 TEP vs. cell coatings

It is important to make a distinction between TEP and the alcian blue-staining cell surface coating that was found during this study. TEP particles, themselves, can be defined as any alcian blue-staining extracellular polymeric particle larger than 0.4 μm. We had expected to detect the increased presence of these particles as a result of increased temperature in a nutrient limited diatom culture. These sticky particles, exuded by diatoms and other organisms during normal growth can stick to cells, causing large aggregates of diatoms to form. What became clear through this experiment was that diatoms exude acid polysaccharides differently. *Chaetoceros muelleri*, instead of ridding itself of acid polysaccharides (APS) to form TEP particles, become coated in APS, allowing the entire surface of the cell to be stained with alcian blue. The *C. muelleri* cells were found stained at various intensities, lying in dense aggregates of cells, presumably stuck together by the sticky coating present even on their spines (Fig. 23). As stated in the results, it is unknown whether the cells amassed into aggregates

because of their sticky surface coating or from the filtering process. However, Fig. 23a shows what appears to be a delicate chain of *C. muelleri* cells stuck together simply through the contact of their spines. This structure may represent a basic unit in *C. muelleri* aggregate formation, first starting as delicate chains and eventually amassing more cells through collisions forming the web-like matrices. Although this is the first known study documenting how *Chaetoceros muelleri* aggregates are comprised almost exclusively of cells and not TEP, identical results were reported in a related species, *Chaetoceros affinis* (Kiorboe and Hansen 1993). A number studies have been conducted to document changes in TEP particles (Kiørboe et al. 1994; Jackson 1995; Passow and Alldredge 1995; Mari 1999; Passow et al. 2001; Thornton 2004; Bhaskar and Bhosle 2006; De La Rocha et al. 2008; Hessen and Anderson 2008; Claquin et al. 2008), however the importance of cell coatings as a fraction of extracellular polymeric substances (EPS) is largely understudied (Thornton 2002).

Through microscopic analysis, APS production in a nitrogen-limited continuous culture did correlate with temperature. As stated above, the presence of APS was rarely detected in TEP and instead was found layering the outside of single cells. This implies that APS detection should be proportional to cell concentration when, in fact, this relationship was not found. Cell concentrations during days 25 to 48 (steady state) only deviated by an average of 6% and correcting APS area for cell concentration still resulted in a significant relationship with temperature. Because images of the stained cells were taken at the same light and exposure levels, observed differences in APS staining intensity were real. Had a cell been heavily coated in APS, it would have

stained darkly and been easily separated from background noise in image analysis. Should a cell have been coated weakly or not at all, the contrast between the cell and the background would result in little or none of the APS being detected through analysis. Intensity levels of staining, however, were not quantified. Colorimetric analysis of TEP has historically been the preferred method for TEP detection but it is clear that this method would greatly misrepresent levels of TEP with *C. muelleri* or any other diatom species that incorporates cell coatings. There are, however, limitations to image analysis of stained APS. Because images were taken with a monochrome camera, chlorophyll and other visible differences in color atop the filter could not be easily separated from the red wavelengths offering intensity of alcian blue staining. Should this analysis be performed in the future, the use of a color CCD camera combined with chlorophyll fluorescence imaging would allow non-blue areas of images to be subtracted before analysis.

LISST analysis of the cultures over time also showed that a positive correlation exists between total volume in a PSD and APS area per cell, possibly implying that should APS area increase, total LISST volume also increases. Net mean changes in LISST PSDs at 22.5°C and 27°C from 20°C show marked and significant changes in volume allocation along the size bin range. Single cell dimension size bins saw a decrease in their volume concentrations, while the large size bins representing aggregates, saw an increase in their volume concentration. Because we were able to show that APS area per cell will increase with changes in temperature to 27°C, increases in aggregate formation at 27°C are most likely resulting from the increase in sticky

particles area present. While it is not clear how each cell becomes coated in APS, as more APS is exuded or coated onto cells, cells are more likely to stick together and form aggregates.

4.5 Diatom physiology and carbon cycling

Coastal diatoms and other phytoplankton are most commonly considered to be under nitrogen limitation or phosphorous limitation while carbon is generally considered to be in excess. In such cases, phytoplankton are often exposed to sunlight and produce the intermediary products of photosynthesis that can't be utilized without nitrogen or phosphorous (Fogg 1983). We do not yet have a full understanding of how diatoms allocate carbon during non-nutrient limited growth let alone nutrient limited growth but are beginning to understand how they treat excess (Geider et al. 1997; Thornton 2002). The overflow hypothesis provides a unique explanation for why phytoplankton appear to "waste" carbon (Thornton 2002; Alderkamp et al. 2007; Hessen and Anderson 2008). It has been proposed that processing excess carbon into the different classes of EPS may have two uses: predation interference and, conversely to what I propose, a method to increase surface area, slowing an individual cells sinking rate (Kiorboe and Hansen 1993; Fukao et al. 2009). However, recent studies indicate that these strategies employed by phytoplankton and prokaryotes, alike, may simply be secondary strategies to the real reason behind carbon excess wastage: preparation of metabolic products for possible future use when a limiting nutrient becomes available again (Russell and Cook 1995; Hessen and Anderson 2008). While these conclusions could not be directly made from our experiments, our results do support our hypotheses. Exposing *Chaetoceros*

muelleri to temperature increase did result in increased APS area which resulted in a measureable shift in its PSD by the formation of large aggregates.

The potential implications on bloom growth and senescence if ocean temperature were to rise would be great with EPS concentration increasing to form more sticky diatoms, more TEP particles, and more dissolved EPS. Higher concentrations of all three classes of EPS would result in greater aggregation of diatoms and other microorganisms. As aggregate number and possibly the size of aggregates in blooms increased, more carbon would sink away from the surface at a faster rate. Diatoms may be responsible for 1/3 of the world's primary production. If diatom blooms, normal phenomenon in spring and fall around the world, were to sink faster, more carbon would be taken away from the surface waters at a faster rate. This would have a large impact not only on the available carbon in the surface waters in terms of POC, DOC, and CO_2 but this larger export could lead to more carbon reaching the ocean floor.

REFERENCES

Agrawal, Y. C. & Pottsmith, H. C. 2000. Instruments for particle size and settling velocity observations in sediment transport. *Marine Geology* 168:89–114.

Agrawal, Y. C., Whitmire, A., Mikkelsen, O. A. & Pottsmith, H. C. 2008. Light scattering by random shaped particles and consequences on measuring suspended sediments by laser diffraction. *Journal of Geophysical Research* 113:23–34.

Alderkamp, A., Buma, A. G. J. & van Rijssel, M. 2007. The carbohydrates of *Phaeocystis* and their degradation in the microbial food web. *Biogeochemistry* 83:99–118.

Andersen, R. A. 2005. *Algal Culturing Techniques*. Academic Press, Boston.

Angles, S., Jordi, A., Garcés, E., Maso, M. & Basterretxea, G. 2008. High-resolution spatio-temporal distribution of a coastal phytoplankton bloom using laser in situ scattering and transmissometry (LISST). *Harmful Algae* 7:808–816.

Behrenfeld, M. J., Halsey, K. H. & Milligan, A. J. 2008. Evolved physiological responses of phytoplankton to their integrated growth environment. *Philosophical Transactions of the Royal Society B: Biological Sciences* 363:2687–2703.

Behrenfeld, M. J., Westberry, T. K., Boss, E. S., O'Malley, R. T., Siegel, D. A., Wiggert, J. D., Franz, B. A., McClain, C. R., Feldman, G. C., Doney, S. C. & others 2009. Satellite-detected fluorescence reveals global physiology of ocean phytoplankton. *Biogeosciences* 6:779–794.

Berges, J. A., Franklin, D. J. & Harrison, P. J. 2001. Evolution of an artificial seawater medium: Improvements in enriched seawater, artificial water over the last two decades. *Journal of Phycology* 37:1138–1145.

Bhaskar, P. V., Grossart, H. P., Bhosle, N. B. & Simon, M. 2005. Production of macroaggregates from dissolved exopolymeric substances (EPS) of bacterial and diatom origin. *FEMS Microbiology Ecology* 53:255–264.

Billett, D. S. M., Lampitt, R. S., Rice, A. L. & Mantoura, R. F. C. 1983. Seasonal sedimentation of phytoplankton to the deep-sea benthos. *Nature* 302:520–522.

Broecker, W. S. 1982. Ocean chemistry during glacial time. *Geochimica et Cosmochimica Acta* 46:1689–1705.

Claquin, P., Probert, I., Lefebvre, S. & Veron, B. 2008. Effects of temperature on photosynthetic parameters and TEP production in eight species of marine microalgae. *Aquatic Microbial Ecology* 51:1–11.

Crocker, K. M. & Passow, U. 1995. Differential aggregation of diatoms. *Marine Ecology Progress Series* 117:249–257.

De Jonge, V. N. 1980. Fluctuations in the organic carbon to chlorophyll a ratios for estuarine benthic diatom populations. *Marine Ecology Progress Series* 2:345–353.

De La Rocha, C. L., Nowald, N. & Passow, U. 2008. Interactions between diatom aggregates, minerals, particulate organic carbon, and dissolved organic matter: further implications for the ballast hypothesis. *Global Biogeochemical Cycle* 22:10–18.

Deuser, W. G. 1970. Isotopic evidence for diminishing supply of available carbon during diatom bloom in Black Sea. *Nature* 225:1069–1070.

DuBois, M., Gilles, K. A., Hamilton, J. K., Rebers, P. A. & Smith, F. 1956. Colorimetric method for determination of sugars and related substances. *Analytical Chemistry* 28:350–356.

Engel, A. 2000. The role of transparent exopolymer particles (TEP) in the increase in apparent particle stickiness (α) during the decline of a diatom bloom. *Journal of Plankton Research* 22:485–497.

Falkowski, P. G. 1998. Biogeochemical controls and feedbacks on ocean primary production. *Science* 281:200–206.

Fogg, G. E. 1983. The ecological significance of extracellular products of phytoplankton photosynthesis. *Botanica Marina* 26:3–14.

Fukao, T., Kimoto, K., Yamatogi, T., Yamamoto, K., Yoshida, Y. & Kotani, Y. 2009. Marine mucilage in Ariake Sound, Japan, is composed of transparent exopolymer particles produced by the diatom *Coscinodiscus granii*. *Fisheries Science* 75:1007–1014.

Gartner, J. 2001. Laboratory and field evaluations of the LISST-100 instrument for suspended particle size determinations. *Marine Geology* 175:199–219.

Geider, R. J., MacIntyre, H. L. & Kana, T. M. 1997. Dynamic model of phytoplankton growth and acclimation: responses of the balanced growth rate and the chlorophyll a:carbon ratio to light, nutrient-limitation and temperature. *Marine Ecology Progress Series* 148:187–200.

Harlay, J., De Bodt, C., Engel, A., Jansen, S., d'Hoop, Q., Piontek, J., Van Oostende, N., Groom, S., Sabbe, K. & Chou, L. 2009. Abundance and size distribution of transparent exopolymer particles (TEP) in a coccolithophorid bloom in the northern Bay of Biscay. *Deep-Sea Research Part I* 56:1251–1265.

Harrison, P. J., Waters, R. E. & Taylor, F. J. R. 1980. A broad spectrum artificial sea water medium for coastal and open ocean phytoplankton. *Journal of Phycology* 16:28–35.

Hessen, D. O. & Anderson, T. R. 2008. Excess carbon in aquatic organisms and ecosystems: physiological, ecological, and evolutionary implications. *Limnology and Oceanography* 53:1685–1696.

Howarth, R. W. & Marino, R. 2006. Nitrogen as the limiting nutrient for eutrophication in coastal marine ecosystems: evolving views over three decades. *Limnology and Oceanography* 51:364–376.

Ivanov, M. V., Lein, A. Y., Miller, Y. M., Yusupov, S. K., Pimenov, N. V., Wehrli, B., Rusanov, I. I. & Zehnder, A. 2000. The effect of microorganisms and seasonal factors on the isotopic composition of particulate organic carbon from the Black Sea. *Microbiology* 69:449–459.

Jackson, G. A. 1995. TEP and coagulation during a mesocosm experiment. *Deep-Sea Research Part II* 42:215–222.

Karp-Boss, L., Azavedo, L. & Boss, E. 2007. LISST-100 measurements of phytoplankton size distribution: evaluation of the effects of cell shape. *Limnology and Oceanography: Methods* 5:396–406.

Kiørboe, T., Lundsgaard, C., Olesen, M. & Hansen, J. L. S. 1994. Aggregation and sedimentation processes during a spring phytoplankton bloom: a field experiment to test coagulation theory. *Journal of Marine Research* 52:297–323.

Kiorboe, T. & Hansen, J. L. 1993. Phytoplankton aggregate formation: observations of patterns and mechanisms of cell sticking and the significance of exopolymeric material. *Journal of Plankton Research* 15:993–1018.

Klaas, C. & Archer, D. E. 2002. Association of sinking organic matter with various types of mineral ballast in the deep sea: Implications for the rain ratio. *Global Biogeochemical Cycle* 16:1116–1030.

Legendre, L. 1990. The significance of microalgal blooms for fisheries and for the export of particulate organic carbon in oceans. *Journal of Plankton Research* 12:681–699.

Leventer, A. 1991. Sediment trap diatom assemblages from the northern Antarctic Peninsula region. *Deep Sea Research Part A. Oceanographic Research Papers* 38:1127–1143.

Li, B., Ward, J. & Holohan, B. 2008. Transparent exopolymer particles (TEP) from marine suspension feeders enhance particle aggregation. *Marine Ecology Progress Series* 357:67–77.

Logan, B. E., Grossart, H. & Simon, M. 1994. Direct observation of phytoplankton, TEP and aggregates on polycarbonate filters using brightfield microscopy. *Journal of Plankton Research* 16:1811–1815.

Mari, X. 1999. Carbon content and C: N ratio of transparent exopolymeric particles (TEP) produced by bubbling exudates of diatoms. *Marine Ecology Progress Series* 183:59–71.

Mari, X. 2008. Does ocean acidification induce an upward flux of marine aggregates? *Biogeosciences* 5:1023–1031.

Menden-Deuer, S., Lessard, E. J. & Satterberg, J. 2001. Effect of preservation on dinoflagellate and diatom cell volume and consequences for carbon biomass predictions. *Marine Ecology Progress Series* 222:41–50.

Monod, J. 1950. La technique de culture continue theorie et applications. *Annales de l'Institut Pasteur* 79:390–410.

Nelson, D. M., Tréguer, P., Brzezinski, M. A., Leynaert, A. & Quéguiner, B. 1995. Production and dissolution of biogenic silica in the ocean: revised global estimates; comparison with regional data and relationship to biogenic sedimentation 9:359–372.

Omta, A. W., Bruggeman, J., Kooijman, S. A. L. M. & Dijkstra, H. A. 2006. Biological carbon pump revisited: feedback mechanisms between climate and the redfield ratio. *Geophysical Research Letters* 33:613–617.

Parsons, T. R., Maita, Y. & Lalli, C. M. 1984. *A Manual of Chemical and Biological Methods for Seawater Analysis*. Pergamon Press, Oxford.

Passow, U. & Alldredge, A. L. 1995. A dye-binding assay for the spectrophotometric measurement of transparent exopolymer particles (TEP). *Limnology and Oceanography* 40:1326–1335.

Passow, U., Shipe, R. F., Murray, A., Pak, D. K., Brzezinski, M. A. & Alldredge, A. L. 2001. The origin of transparent exopolymer particles (TEP) and their role in the sedimentation of particulate matter. *Continental Shelf Research* 21:327–346.

Piontek, J., Händel, N., Langer, G., Wohlers, J., Riebesell, U. & Engel, A. 2009. Effects of rising temperature on the formation and microbial degradation of marine diatom aggregates. *Aquatic Microbial Ecology* 54:305–318.

Rienecker, E., Ryan, J., Blum, M., Dietz, C., Coletti, L., Marin, I. I. I. & Bissett, W. P. 2008. Mapping phytoplankton in situ using a laser-scattering sensor. *Limnology and Oceanography: Methods* 6:153–161.

Russell, J. B. & Cook, G. M. 1995. Energetics of bacterial growth: balance of anabolic and catabolic reactions. *Microbiological Reviews* 59:48–62.

Sarthou, G., Timmermans, K. R., Blain, S. & Treguer, P. 2005. Growth physiology and fate of diatoms in the ocean: a review. *Journal of Sea Research* 53:25–42.

Schartau, M., Engel, A., Schröter, J., Thoms, S., Völker, C. & Wolf-Gladrow, D. 2007. Modelling carbon overconsumption and the formation of extracellular particulate organic carbon. *Biogeosciences* 4:433–454.

Seinfeld, J. H. & Pandis, S. N. 1997. *Atmospheric Chemistry and Physics: From Air Pollution to Climate Change*. Wiley-Interscience, New York.

Serra, T., Colomer, J., Cristina, X. P., Vila, X., Arellano, J. B. & Casamitjana, X. 2001. Evaluation of laser in situ scattering instrument for measuring concentration of phytoplankton, purple sulfur bacteria, and suspended inorganic sediments in lakes. *Journal of Environment Engineering - ASCE* 127:1023–1030.

Smetacek, V. S. 1985. Role of sinking in diatom life-history cycles - ecological, evolutionary and geological significance. *Marine Biology* 84:239–251.

Strickland, J. & Parsons, T. 1984. *A Practical Handbook of Seawater Analysis*. Fisheries Research Board of Canada, Ottawa.

Thornton, D. & Thake, B. 1998. Effect of temperature on the aggregation of *Skeletonema costatum* (Bacillariophyceae) and the implication for carbon flux in coastal waters. *Marine Ecology Progress Series* 174:223–231.

Thornton, D. 2002. Diatom aggregation in the sea: mechanisms and ecological implications. *European Journal of Phycology* 37:149–161.

Thornton, D. 2004. Formation of transparent exopolymeric particles (TEP) from macroalgal detritus. *Marine Ecology Progress Series* 282:1–12.

Thornton, D., Fejes, E. M., DiMarco, S. F. & Clancy, K. M. 2007. Measurement of acid polysaccharides in marine and freshwater samples using alcian blue. *Limnology and Oceanography: Methods* 4:73–87.

Treguer, P. & Pondaven, P. 2000. Global change - Silica control of carbon dioxide. *Nature* 406:358–359.

Wohlers, J., Engel, A., Zöllner, E., Breithaupt, P., Jürgens, K., Hoppe, H., Sommer, U. & Riebesell, U. 2009. Changes in biogenic carbon flow in response to sea surface warming. *Proceedings of the National Academy of Sciences* 106:7067–7072.

Zack, G., Rogers, W. & Latt, S. 1977. Automatic measurement of sister chromatid exchange. *Journal of Histochemistry and Cytochemistry* 25:741–753.

APPENDIX I

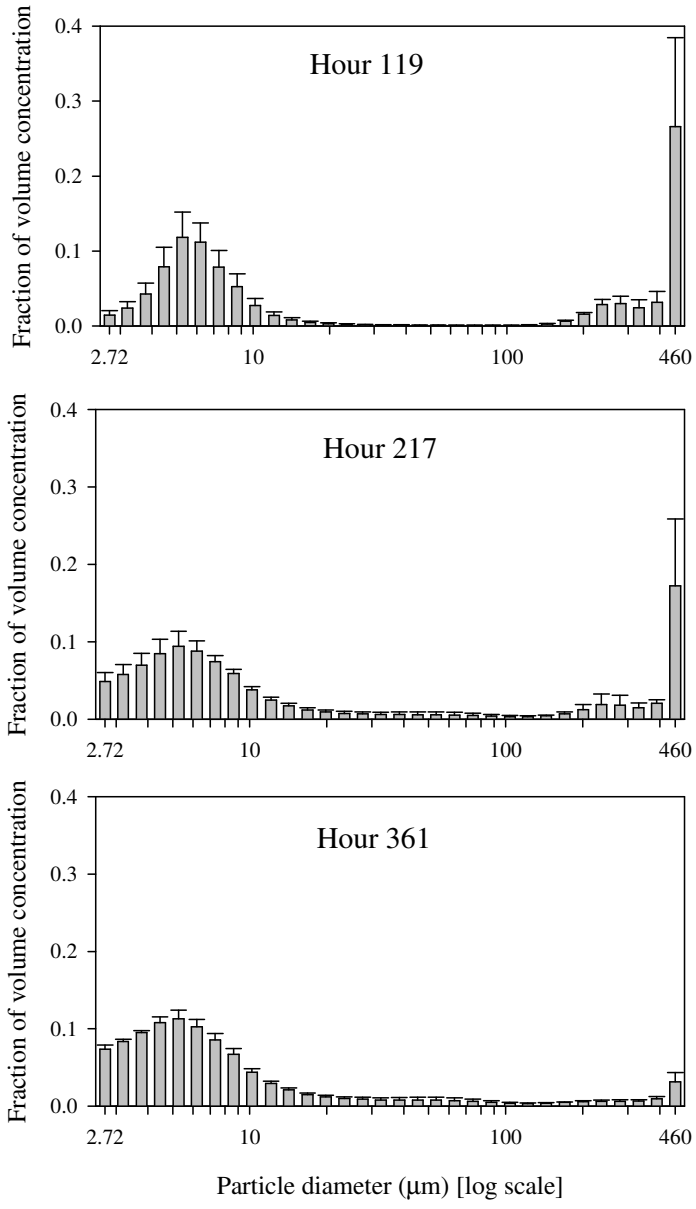

Fig. A1. Particle size distribution (PSD) of *Thalassiosira weissflogii* during batch culture experiment. Panels represent the PSDs for sample days 1, 2, and 3. Bars represent the fraction of total volume concentration (mean + SD; n = 3). See Fig. 6 for growth curve.

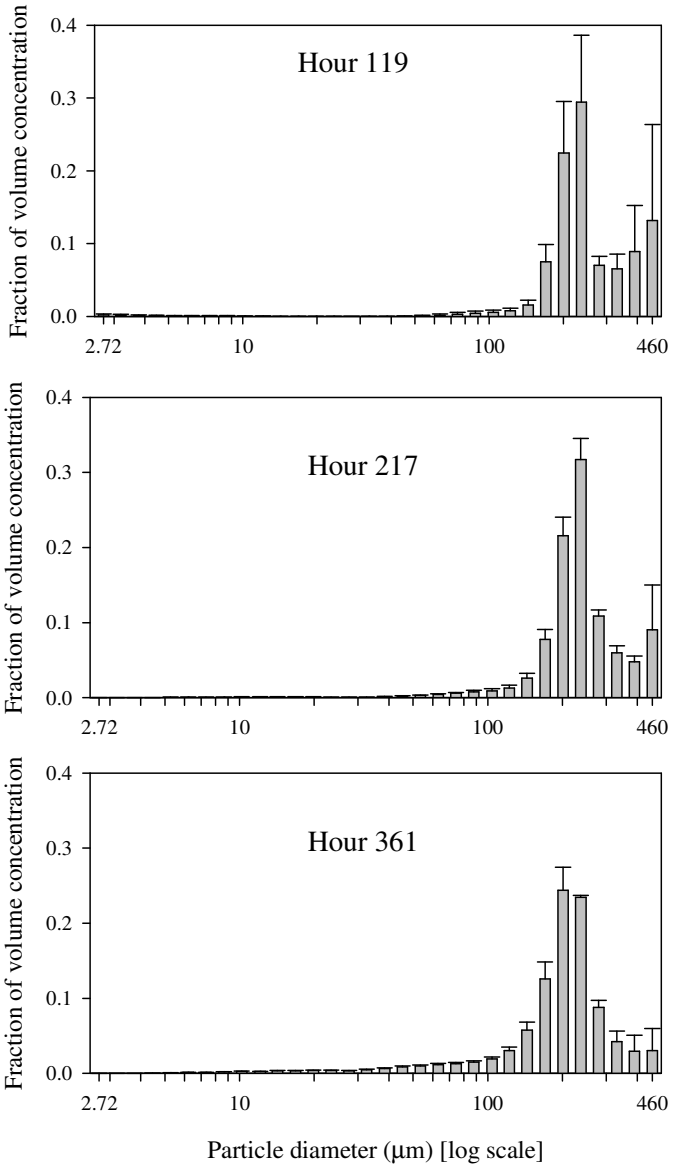

Fig. A2. Particle size distribution (PSD) of *Coscinodiscus wailesii* during batch culture experiment. Panels represent the PSDs for sample days 1, 2, and 3. Bars represent the fraction of total volume concentration (mean + SD; n = 3). See Fig. 7 for growth curve.

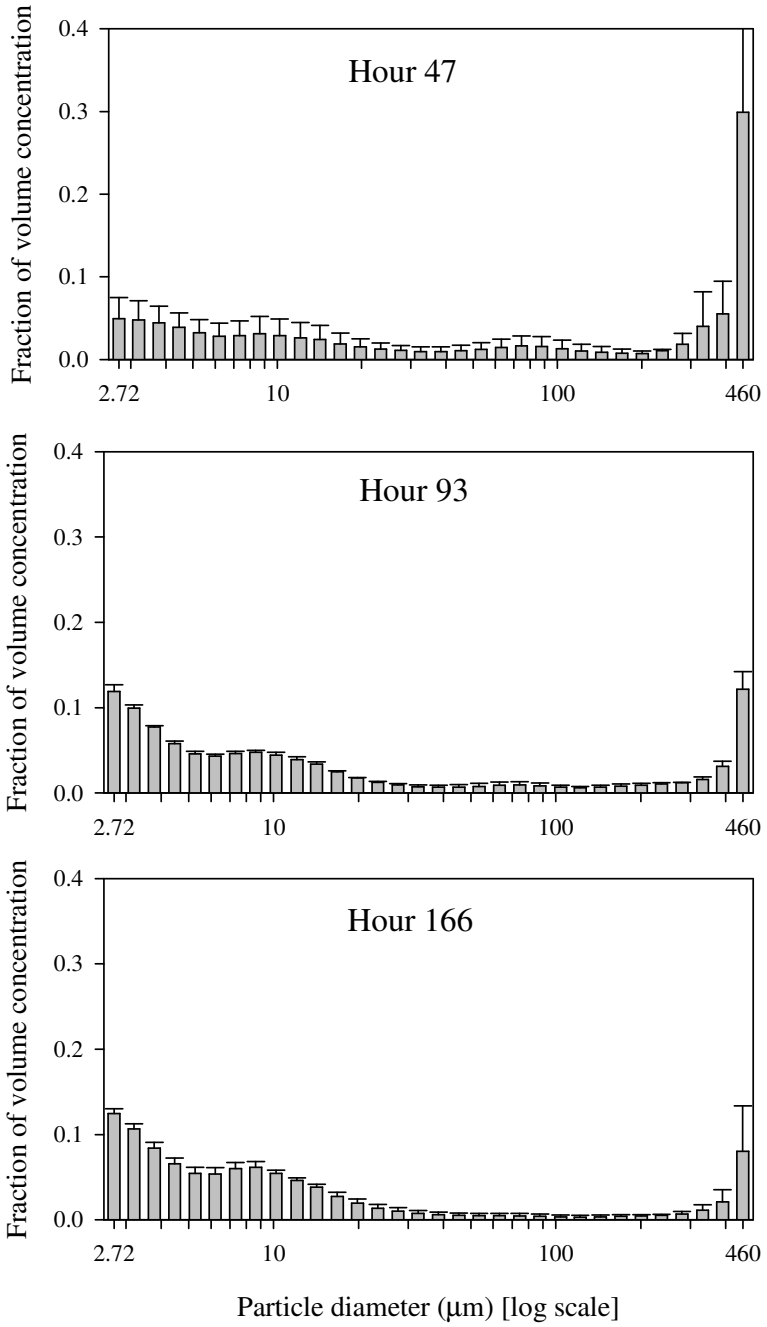

Fig. A3. Particle size distribution (PSD) of *Phaeodactylum tricornutum* during batch culture experiment. Panels represent the PSDs for sample days 1, 2, and 3. Bars represent the fraction of total volume concentration (mean + SD; n = 3). See Fig. 9 for growth curve.

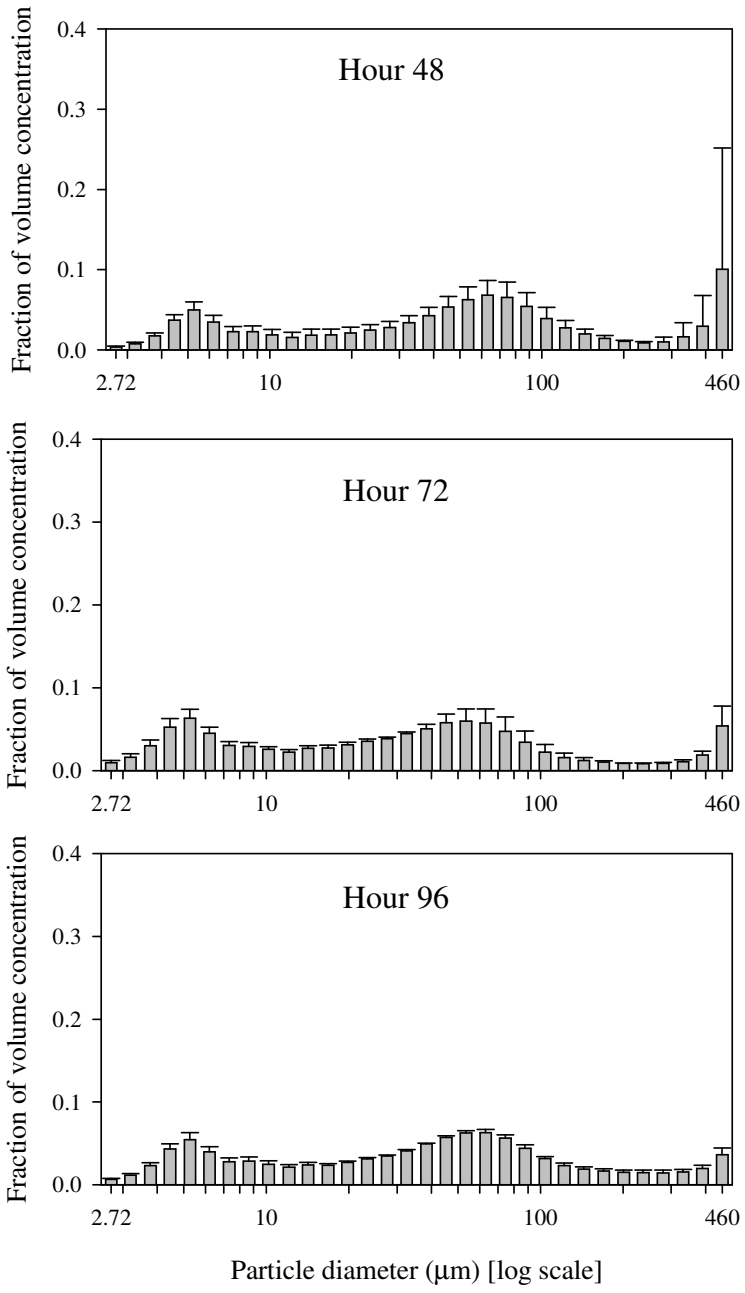

Fig. A4. Particle size distribution (PSD) of *Skeletonema costatum* during batch culture experiment. Panels represent the PSDs for sample days 1, 2, and 3. Bars represent the fraction of total volume concentration (mean + SD; n = 3). See Fig. 10 for growth curve.

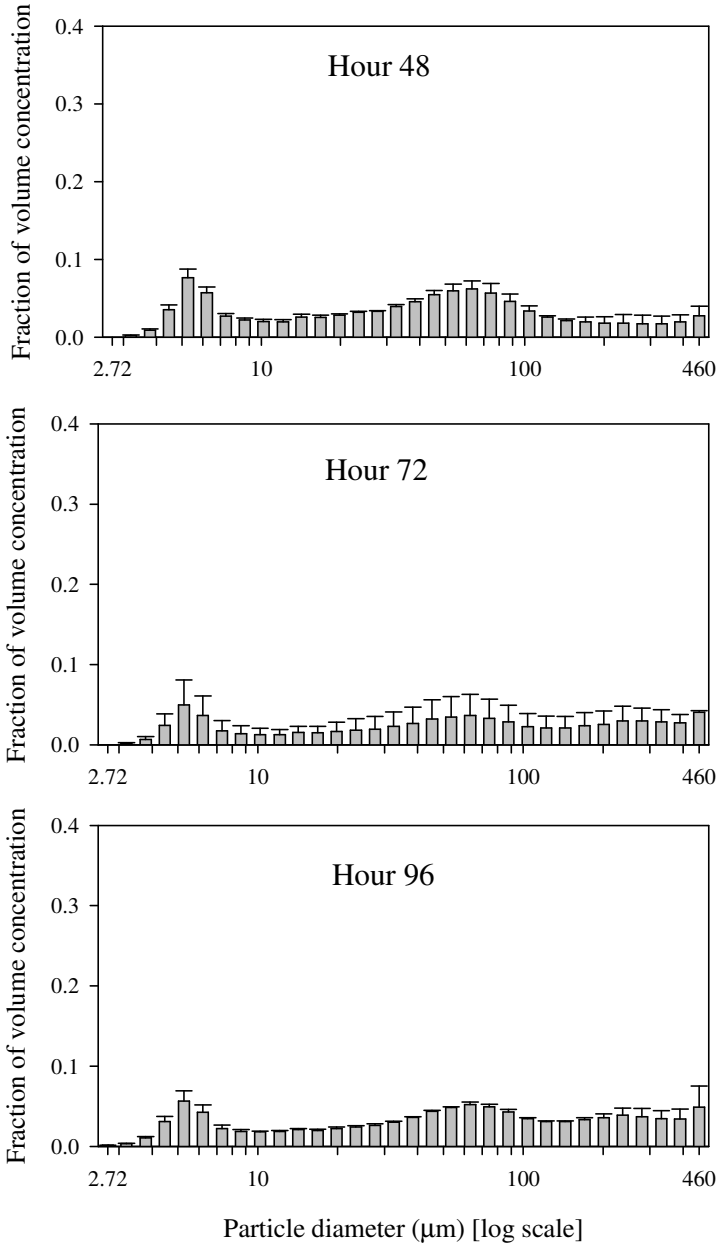

Fig. A5. Particle size distribution (PSD) of *Skeletonema marinoi* during batch culture experiment. Panels represent the PSDs for sample days 1, 2, and 3. Bars represent the fraction of total volume concentration (mean + SD; n = 3). See Fig. 11 for growth curve.

VITA

Name:	Charles Edward Rzadkowolski
Address:	Charles Rzadkowolski 3146 TAMU College Station, TX 77843 - 3146
Email address:	cerzadko@gmail.com
Education:	B.S. Biology, B.S. Marine Science, Coastal Carolina University, 2007 M.S. Oceanography, Texas A&M University, 2010